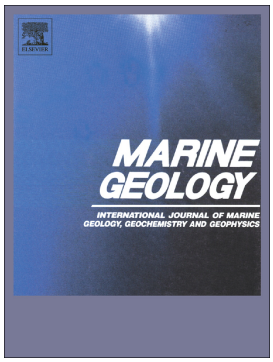

Ice-stream dynamics of the SW Barents Sea revealed by high-resolution 3D seismic imaging of glacial deposits in the Hoop area

B. Bellwald, S. Planke, E.D. Piasecka, M.A. Matar, K. Andreassen

PII: S0025-3227(17)30275-X
DOI: doi:10.1016/j.margeo.2018.03.002
Reference: MARGO 5770

To appear in: *Marine Geology*

Received date: 1 June 2017
Revised date: 16 November 2017
Accepted date: 1 March 2018

Please cite this article as: B. Bellwald, S. Planke, E.D. Piasecka, M.A. Matar, K. Andreassen , Ice-stream dynamics of the SW Barents Sea revealed by high-resolution 3D seismic imaging of glacial deposits in the Hoop area. The address for the corresponding author was captured as affiliation for all authors. Please check if appropriate. Margo(2017), doi:10.1016/j.margeo.2018.03.002

Ice-stream dynamics of the SW Barents Sea revealed by high-resolution 3D seismic imaging of glacial deposits in the Hoop area

Bellwald, B.[1,2], Planke, S.[1,3], Piasecka, E.D.[4], Matar, M.A.[1,5], Andreassen, K.[4]

[1]Volcanic Basin Petroleum Research (VBPR) AS, Oslo Science Park, Gaustadalléen 21, N-0349 Oslo, Norway (benjamin@vbpr.no)

[2]Department of Earth Science, University of Bergen, Allégaten 41, N-5007 Bergen, Norway

[3]Centre for Earth Evolution and Dynamics (CEED), University of Oslo, Sem Sælands vei 1, N-0371 Oslo, Norway

[4]CAGE, Centre for Arctic Gas Hydrate, Environment and Climate, UiT The Arctic University of Norway, N-9019 Tromsø, Norway

[5]Nordic Geo-Consult AS, Gamle Drammensvei 77, N-1369 Bærum, Norway

Abstract

Recent developments in seismic acquisition systems and seismic data visualization have contributed to improve the imaging of seismic geomorphologies over a broad range of topics. This study focuses on a new high-resolution P-Cable 3D seismic cube located in the Hoop area in the SW Barents Sea. The scientific motivations of the study are (1) to document glacial landforms on a meter-scale, (2) to study the link of these landforms with the subsurface, and (3) to understand ice-stream dynamics by detailed interpretation of main horizons, including the seabed, intra-glacial horizons, and Upper Regional Unconformity (URU). The horizons are assessed using the concept of seismic geomorphology, and compared with interpretations derived from conventional 3D seismic and state-of-the-art multibeam echosounder technologies to discuss the benefits and limitations of the different geophysical technologies. A well-defined intra-glacial seismic reflection is imaged in the eastern part of the P-Cable cube. This reflection has an overall NE-trending ridge-shaped morphology, which is up to 50 meters high and 5-10 km wide, and interpreted as a shear margin moraine. The top of the moraine displays well-defined iceberg ploughmarks and clear slope failure events along its eastern flank. The seabed geomorphology, which has been directly shaped by glacial processes related to multiple phases of ice streaming, appears to be influenced by the buried shear margin moraine. Mega-scale glacial lineations (MSGLs) indicative of fast-flowing ice streams characterize the seabed west of the moraine. Infilled MSGLs and different sets of iceberg ploughmarks with large berms dominate the seabed geomorphology above the moraine. The seabed east of the moraine, characterized by a smooth morphology and few pockmarks, is inferred to reflect more slowly-moving ice. Not resolved by other geophysical techniques, seismic attribute maps of P-Cable 3D allowed the identification of smaller ploughmarks and corrugated ridges related to paleo tides. Eroded by the larger iceberg ploughmarks, these small ploughmarks are suggested to be linked to an earlier rapid disintegration of the Barents Sea Ice Stream. The new high-resolution 3D seismic data have led to the development of a revised ice-stream model of the Barents Sea, linking the glacial deposits to different ice stream events.

Keywords: *High-resolution 3D seismic – Barents Sea – Shear margin moraine – Mega-scale glacial lineations – Iceberg ploughmarks*

1. Introduction

Acoustic methods based on marine echo-sounding principles are currently the most widely used techniques for mapping submarine glacial landforms (Jakobsson et al., 2016). Bathymetric data for such studies are typically collected by multibeam echosounders, with frequencies varying from 12 to 500 kHz (www.km.kongsberg.com), providing high-resolution geomorphology along a swath. Sub-bottom profilers are echosounders designed to penetrate the seabed and usually operate with frequencies in the range of 1 to 20 kHz. Their penetration is up to about 100 m in soft and low-absorbing sediments, but commonly only several tens of meters in previously glaciated environments (Jakobsson et al., 2016; Bellwald et al., 2016). While sub-bottom profiler data give valuable information of the uppermost sediment package, seismic reflection profiling is designed for deeper stratigraphy. The two main types of seismic reflection mapping are based on 2D and 3D data, generally in the frequency range of 50 to 200 Hz (Trabant, 1984). 2D seismic methods acquire data along profiles, whereas 3D seismic methods acquire data in a regular and closely-spaced grid.

High-resolution P-Cable 3D seismic data have successfully been acquired in numerous marine surveys worldwide, helping to solve problems related to slope stability (Crutchley et al., 2012), pore pressure phenomena (Plaza-Faverola et al., 2011), and seismicity (Nishenko et al., 2012). This technology has also been used for imaging of iceberg ploughmarks in the SW Barents Sea with resolution comparable to multibeam swath-bathymetric images (Vadakkepuliyambatta et al., 2016). However, little effort has been undertaken to systematically evaluate the potential of such data for high-resolution mapping and imagery of well-preserved glacial landforms and their link with the underlying geology.

Here we use surfaces and sequences interpreted in P-Cable 3D seismic data, originally collected for petroleum investigations, and compare them with structures mapped by conventional seismic data. About 13,000 km^2 of the seabed geomorphology of the study area has previously been mapped based on conventional 3D seismic data with a bin size of 12.5x18.75 m (Piasecka et al., 2016), revealing several sets of mega-scale glacial lineations and iceberg ploughmarks scouring the seabed.

The aim of this study is to map recent glacial deposits and to investigate the effect of a paleo-ice stream on the paleo-seabed and the underlying glacial strata using P-Cable data. The study is based on

the concept of seismic geomorphology, i.e. the extraction of landform geometries using predominantly three-dimensional seismic data (Posamentier et al., 2007), which can resolve meter-scale subglacial landforms and study the potential relation of these landforms with the subsurface geology. By characterizing glacial structures along different surfaces, we can evaluate in what detail the different glacier-related features can be identified. In addition, we improved the visualization of meter-scale glacial deposits using seismic attribute analysis.

Intraglacial reflections not visible in conventional seismic data and meter-scale glacial structures identified in this study contribute to improving the glacial history of the region and to better understand glacio-erosive processes in existing models. This study is also a valuable contribution for the comparison of geophysical techniques currently used in marine studies. The results of the detailed mapping of buried glacial deposits may further be considered for planning boreholes and installing seabed infrastructure. Conclusions on processes identified in this study should further be applicable to modern glaciated areas, such as the West Antarctic Ice Sheet.

2. Glaciological framework

The Barents Sea is <500 m deep and extends over one of the widest continental shelves in the world. It is characterized by shallow banks and several overdeepened cross shelf troughs, with Bjørnøyrenna (Bear Island Trough) as the most prominent one (Fig. 1a). During the Last Glacial Maximum the Barents Sea was entirely covered by the ~2200 m-thick Barents Sea Ice Sheet, with the Bjørnøyrenna Ice Stream as the main drainage outlet (Siegert and Dowdeswell, 1996; Svendsen et al., 2004; Patton et al., 2016). The seabed of the Barents Sea has been intensively eroded during the late Cenozoic time period by repeated glaciations. This erosion led to the deposition of the ~3500 m-thick Bear Island Trough Mouth Fan (TMF) and the ~4000 m-thick Storfjorden TMF on the western Barents Sea margin (Fig. 1a) (Vorren et al., 1991; Fiedler and Faleide, 1996; Faleide et al., 1996; Vorren et al., 1998; Laberg et al., 2012). The continental shelf is covered by a thin (generally <100 m) Quaternary sediment package (Solheim and Kristoffersen, 1984; Sættem et al., 1992; Vorren et al., 1992; Vorren and Laberg, 1997). Less than 2 m of Holocene sediments are covering most of the Barents Sea

(Elverhøi and Solheim, 1984). However, details on the changing extent of the Scandinavian Ice Sheet are poorly documented in the Barents Sea (Hughes et al., 2016). Grounding zone wedges, retreat moraines and different sets of lineations document episodic readvances and stillstands during the deglaciation of the Barents Sea Ice Sheet (Winsborrow et al., 2010; Andreassen et al., 2014; Bjarnadóttir et al., 2014). According to few existing radiocarbon dates, the last major deglaciation started in the southwest at ~16.9 ka BP (Rüther et al., 2011), and was followed by stepwise retreat of Bjørnøyrenna to a location east of Svalbard by ~11.3-12.0 ka BP (Salvigsen, 1981; Rüther et al., 2017) (Fig. 1a).

A buried paleo-seabed surface corresponds to a prominent erosional unconformity in the Barents Sea, called Upper Regional Unconformity (URU). URU separates underlying westward-dipping stratified sedimentary rocks from the horizontally deposited Quaternary sediments (Solheim and Kristoffersen, 1984; Vorren et al., 1986; Solheim et al., 1996). URU lies at a depth of approximately 40-60 m below the contemporary seabed in the study area (Sættem et al., 1992; Piasecka et al., 2016). URU represents the erosional base for several subsequent continental shelf glaciations, and the sediments deposited atop URU record the cycles of advances and retreats of the Barents Sea Ice Sheet (Vorren et al., 1990; Sættem et al., 1992). Ice stream flow-sets on URU and the seabed indicate that the area has been affected by highly dynamic ice streams of variable flow orientation (Piasecka et al., 2016) (Fig. 1b).

The Bjørnøyrenna is crosscut by two large fault complexes along its axis: the Bjørnøyrenna Fault Complex in the south and the Hoop Fault Complex in its central part (Sigmond, 1992). The study area of this work is located over the Hoop Fault Complex at water depths of ~450 m at 73-75° N and 22-26° E. The structural setting of the study area is characterized by a series of long-lived faults, which were most likely reactivated periodically since the Carboniferous (Sigmond, 1992; Sættem et al., 1994). Reservoir rocks occur here at shallow water depths of less than ~400 m below seabed, and high-resolution seismic techniques have significantly contributed to mapping the distribution of these shallow petroleum reservoirs (Widmaier et al., 2017). Several commercial discoveries in Jurassic rocks made the SW Barents Sea among one of the most prospective areas (Fig. 1b) (Henriksen et al., 2011; www.npd.no).

3. Data and methods

3.1 Data

The used P-Cable 3D seismic data cover ~200 km^2 (21 x 11 km, 73-74 ˚N/ 24-26 ˚E) in the Hoop area in water depths between 430 and 490 m (Fig. 1b). The P-Cable technology used for this study consists of 16 streamers, which are 25 m in length with 8 geophones per streamer and attached to a cross cable towed perpendicular to the direction of the vessel (Planke et al., 2009; www.pcable.com). The seismic data were acquired in 2014 using a 300 in^3 airgun array at 2.5 m water depth, 2 s recording length, 0.5 ms sampling interval, a streamer separation of 9.5 m and a bin size of 6.25x4.75 m. The minimum distance between source and receiver is c. 120 m. The streamer positions have been calculated based on a GPS on the vessel and one GPS per paravane.

The maximum frequency of the P-Cable 3D seismic data decreases from 325 Hz at the seabed to ~300 Hz at the base of the Quaternary sediment package, with a vertical resolution of 1-5 m and a horizontal resolution of 2-10 m. The horizontal and vertical resolution of the P-Cable 3D are up to eight times higher than the 12.5x18.75 m bin size of the conventional 3D seismic data (Figs. 2, 3). The data were provided by TGS, VBPR and WGP. After the seismic survey, the data have been processed as a 3D seismic volume and migrated by TGS and DECO.

A total of 37 gravity cores have been collected along a 41 km-long sampling profile crossing the P-Cable cube (Fig. 1b). The site spacing of the 58-226 cm-long cores varies from 700 to 2000 m. These sediment cores have been logged to add ground-truth to the geophysical information provided by the seismic data.

Along the sampling profile, bathymetric data have been collected using a Reson SeaBat 7111 multibeam echosounder, which is built to operate in water depths from 3 to 1000 m. Operating at 100 kHz, the system forms 101, 201 high-density equi-angle or 301 equi-distant beams to cover a total receive sector of 150˚ (www.seafloorsystems.com). Bathymetric data and interpretations on

conventional 3D seismic data have been used to compare imaging of subglacial landforms using P-Cable 3D technology (Fig. 3).

3.2 Seismic interpretation

Interpretation of the high-resolution 3D seismic data was performed in Kingdom v. 2014 and Petrel v. 2016. Three seismic horizons have been picked throughout the cube (Figs. 2 and 4; Tab. 1): (i) the seabed reflection as the first positive-amplitude reflection for all 2500 inlines, located in water depths of 430 m (570 ms) to 485 m (645 ms), (ii) Upper Regional Unconformity (URU) as a positive-amplitude reflection in depths of 640-680 ms and (iii) a ridge-shaped feature as the most prominent positive-amplitude reflection within the Quaternary sediment package in depths of 590 to 680 ms, hereafter referred to as the Top moraine. URU and Top moraine have been picked for every 10th inline throughout the cube and up to every second inline in selected areas. Gridded surfaces have been generated to analyze the seismic geomorphology and to correlate the identified subglacial landforms with the underlying geology. Furthermore, isopach maps of different sediment packages have been created (Fig. 5a). A constant velocity of 1500 m/s was used for the depth conversions. Challenges in picking horizons included numerous grooves on the seabed, occasional irregularities of the URU reflection and the weak reflection defining the Top moraine (Fig. 4). The P-Cable technology improved geomorphological mapping of intra- and base-glacial horizons, not resolved in conventional seismic data (Fig. 2).

Although a seismic trace consists of multiple components (time and amplitude), seismic interpretation of geomorphic features is often based on time. Here we analyze the different components as single attributes and in combination (multi-attribute analysis) to detect and image geological patterns with high quality and minimal influence of the interpreter. Seismic attribute analysis provides more details of the different glacial landforms and information on the processes involved in their formation (Fig. 5b). The curvature and quadratic amplitude attributes have been used to image meter-scale ploughmarks and corrugation ridges. These attributes are most suitable to identify small-scale glacial landforms. The dip attribute is applied to image flanks and troughs of glacial landforms. Variance has

been used as an attribute to image sediment reworking. We assume that the waveforms of traces adjacent over a specific window differ between reworked sediment and troughs eroded by icebergs.

3.3 Technology comparisons

High-resolution 3D seismic technologies are developed to deal with the challenging combination of shallow water and shallow exploration targets, which cannot be sufficiently addressed by the application of conventional marine seismic acquisition and imaging techniques (Widmaier et al., 2017). We analyze conventional datasets of both multibeam echosounder (MBE) and 3D seismic systems (Tab. 2), even if instrument and survey designs can be more sophisticated for specific datasets that are not discussed in this study. Echosounders developed to suite autonomous underwater vehicles or remotely operated vehicles, and dual-gun P-Cable 3D systems, are capable of imaging the seabed with higher resolution than conventional systems. The comparisons are done along a MBE swath crossing the P-Cable cube (Fig. 3a), assuming a water depth of 450 m and a propagation velocity of 1500 m/s in water (Tab. 2).

Resolution means the minimum distance by which two features must be separated to be recorded as distinct entities **(**Sheriff, 1997**)**. Vertical resolution is the ability to distinguish individual reflecting surfaces, and is defined by different limits. The Rayleigh resolution limit (Kallweit and Wood, 1982) is $\lambda/4$, whereas the Widess limit is $\lambda/8$, where λ is the dominant wave length. The vertical resolution is normally defined as a quarter of a wavelength or less. Geological features observed at the seabed and on buried horizons thus represent a depth interval of at least a quarter of a wavelength above and below the mapped surfaces. The Reson SeaBat 7111 and the Kongsberg EM 300 MBE systems vertically resolve structures in a centimeter-scale (Tab. 2). Conventional and P-Cable 3D seismic technologies vertically resolve structures on a meter-scale, and have a lower vertical resolution than MBE data. However, the vertical resolution of MBE systems is limited to the seabed surface, whereas 3D seismic data additionally resolve buried structures.

The horizontal resolution, the ability to distinguish separate features on a horizon, is often defined by the width of the first Fresnel Zone (Leenhart, 1972; Sheriff, 1997; Brown, 1999). The horizontal resolution is calculated to c. 3 m for these MBE systems. As 3D seismic data can be migrated, their horizontal resolution equals a quarter of the wave length, making horizontal resolution of 3D seismic technologies comparable to MBE systems.

The advantage of the P-Cable technology compared to MBE systems is the number of short offset traces, the low-angle data collection and the close spacing without interpolation. Thereby geological structures such as boulders and pockmarks can horizontally be resolved in high-resolution (Fig. 3). These structures can generate shadow zones in MBE data. In shallow waters, such as the Barents Sea, traditional MBE systems collect data with a sailing-line distance of ~1000 m and an opening angle of 45˚ on both sides. An average sailing line of 70 m in P-Cable 3D allows low-angle data collection. The fold of a P-Cable system with a bin size of 6.25x4.75 m is calculated to 4. Stacking four traces in P-Cable data allows to reduce the signal-to-noise ratio, and to average identified structures.

4. Surfaces

4.1 Seabed

The slightly inclined seabed is located in water depths varying between ~490 m (645 ms) in the southwest and ~430 m (570 ms) in the southeastern part of the study area (Fig. 6a). The morphology of the seabed can be separated into three distinct zones characterized by (i) elongated linear ridge-groove features (Zone I), (ii) curvilinear grooves cutting into linear ridge-groove features (Zone II), and (iii) relatively flat seabed with a few curvilinear grooves and circular depressions (Zone III) (Fig. 7). Some of these seabed features are occasionally rimmed. Linear and curvilinear grooves appear in all water depths, but may dominate different zones. The sediments of the gravity cores are characterized by soft silty clays with a brownish to grayish color and occasional sandy interlayers. Their physical properties vary from water-saturated to stiff and compacted.

Zone I is located in the western part of the cube in water depths of 450 to 490 m (Figs. 6, 7). The sub-seabed sediment package is characterized by low-amplitude reflections, has a maximum thickness of 50 m (Fig. 8), and the cores penetrate down to 1.3 m in average. The seabed of Zone I is dominated by mega-scale glacial lineations (MSGLs), which are occasionally crosscut by iceberg ploughmarks and one large pockmark (Fig. 7b). Smaller iceberg ploughmarks often contain internal corrugated ridges, and follow the troughs of the MSGLs (Fig. 7c). The pathway of the most prominent iceberg, whose ploughmark can be traced into Zone II, shows indications of break-up in Zone I (Fig. 9). Towards the west, this iceberg eroded almost down to URU (21 m of Quaternary sediments) and formed a ploughmark with meter-high rims (Figs. 9b, 9c).

Zone II is dominated by cross-cutting iceberg ploughmarks, iceberg pits and a large pockmark (Figs. 6, 7). While having lower levels of erosion compared to Zone I (Profile A in Fig. 9b), the sinuosity of iceberg ploughmarks is here highest (Fig. 7b). Ploughmarks are laterally vanishing and infilling the MSGLs in this zone, resulting in less pronounced and sometimes even completely erased MSGLs (Fig. 8). The MSGLs in Zone II tend to be wider and shallower (Fig. 8), having a different morphology compared to those in Zone I. The Quaternary sediment package, around 20-65 m thick, is characterized by one internal, positive, high-amplitude reflection, which seems to be the limit for glacio-erosive processes along the seabed (Figs. 8, 9). The sediment cores in Zone II penetrate to a depth of 1.6 m in average.

Zone III is characterized by a relatively smooth, flat seabed covering 20 km^2 in the southeastern part of the cube, where the water depths are shallowest (430-440 m) (Figs. 6, 7). The underlying 50-60 m-thick Quaternary sediment package is dominated by negative, acoustically semi-continuous reflections (Fig. 8b). Besides some iceberg ploughmarks, several smaller pockmarks appear in this zone (Fig. 7b). The core penetration depth is here longest, with an average penetration depth of 2.0 m.

4.2 Buried ridge-shaped structure

The intraglacial sediment package is characterized by a weaker and discontinuous positive-amplitude reflection within the Quaternary sediments (Fig. 4, yellow line). This reflection, mapped in depths of

440 (590 ms) to 510 m (680 ms), is buried by up to 40 m of sediment and occasionally almost reaching the seabed.

Gridding of this reflection reveals a positive relief, ridge-shaped structure (Figs. 6b, 10), with elevations of up to 50 m above the surrounding terrain. The flanks of the ~5-10 km-wide structure have slope gradients of ~4° in the west and ~10° in the east. The internal geometry of the ridge is characterized by steeply-dipping reflections with positive amplitudes. Wedges deposited on top of URU onlap these steeply-dipping reflections at their base (Fig. 10c). Several ~20 m-thick and up to 1500 m-long wedges, with acoustically chaotic facies, onlap the southeastern flank of the ridge-shaped structure.

The seabed is not cutting into this reflection. However, iceberg ploughmarks and MSGLs identified at the top of the ridge-shaped feature indicate that it has been exposed to glacial erosion at one or multiple earlier glacial events (Fig. 10). The iceberg ploughmarks are aligned parallel to the ridge axis in semi-linear sets of grooves, which are 250-400 m wide and 10-20 m deep. Seismic interpretation suggested imprints from multi-keel iceberg ploughing on the ridge (Fig. 11). The MSGLs, less pronounced landforms compared to the ploughmarks, are characterized by NNE-SSW- and N-S-oriented linear grooves. An 1100 m wide trough, characterized by a continuous high-amplitude reflection and the same orientation as the semi-linear grooves, shapes the ridge in its central part (Fig. 10).

4.3 Upper Regional Unconformity (URU)

URU, mapped in depths of 480 m (640 ms) to 510 m (680 ms) (Fig. 6c), is overlain by a 20-65 m-thick Quaternary sediment package characterized by mainly low-amplitude reflections (Fig. 4). The main structures include several NW-SE-propagating channels along a 1200-2300 m-wide major depression in the northeastern part of the study area. A 3 m-high, 2000-2500 m-wide NE-SW-oriented topographic high shapes URU in the southeastern part of the study area.

URU displays linear and curvilinear E-W to NNE-SSW-oriented grooves (Fig. 6c). The position of the largest pockmark of the seabed is correlating with a groove on URU. Minor glacial landforms further include circular- to oval-shaped depressions with occasional rims in the SSW of the depressions.

5. Seismic geomorphology

This section describes the seismic geomorphology of small-scale seabed expressions, and discusses the sedimentary processes involved in their erosional and depositional behavior afterwards.

Mega-scale glacial lineations (MSGLs)

Description: Long, elongated linear ridge-groove features have been mapped over large areas of the seabed, with water depths >440 m (Figs. 6, 7). These 300-900 m wide features are 12-18 m high from crest to trough (Fig. 8), with dips of 2-10° along the lateral edges of the grooves (Fig. 5b). Most of these linear features comprise a groove with a small ridge on each side, and can be grouped into a NE-SW oriented set cutting into a NNE-SSW oriented set of elongated lineations (Fig. 7b).

Interpretation: We follow the interpretation of similar features in other areas and suggest these linear, wide and shallow ridge-groove features represent mega-scale glacial lineations (MSGLs) (Ó Cofaigh et al., 2005; Ottesen et al., 2005; Shaw et al., 2006; Jakobsson et al., 2011). MSGLs have been formed subglacially by grounded fast-flowing ice streams (Clark et al., 2003) and subglacial sediment deformation (e.g. Tulaczyk et al., 2001; Clark, 1993). MSGLs observed in Antarctica show depths of a few meters and widths of tens of meters to a few hundred meters (Ó Cofaigh et al., 2002; Dowdeswell et al., 2008). Different sets of streamlined subglacial landforms are inferred to record different events of past ice-flow of the Bjørnøyrenna Ice Stream (Andreassen and Winsborrow, 2009). The MSGL sets identified in our study area have recently been mapped among other, E-W to NNE-SSW directed, flow-sets of fast-flowing ice streams (Piasecka et al., 2016).

Iceberg ploughmarks

Description: Chaotically-oriented grooves abundantly occur in all water depths and can be traced for several kilometers (Figs. 6, 7). The 50-400 m wide grooves overprint and crosscut both MSGLs and curvilinear grooves (Fig. 8) without completely erasing them. Occasionally associated with 2-6 m high asymmetric marginal berms, they erode down to 20 m and form V- to U-shaped cross profiles with multiple furrows (Figs. 8, 9). The flat-bottomed troughs have flanks with dip angles of 10-25° (Fig. 5b). The grooves are wider (300-400 m) downstream towards their termini, where they also form their highest rims (Fig. 9). The rims of these grooves show high variance values (vertical window of 5 ms in seismic data), whereas an absence of rims correlates with lower variance values (Fig. 12).

The curvilinear grooves can be grouped into two types: A first group is characterized by 100-300 m wide, 3-6 m deep and several kilometer long grooves (Fig. 7b). Most of these curvilinear grooves in Zone III are rimmed all along their paths. Towards their termini, the grooves are 15-20 m deep, 300-400 m wide and surrounded by up to 6 m high rims (Figs. 9, 12). Occasionally the grooves end in several meter deep circular depressions and a terminal berm (Fig. 12).

The second group of curvilinear grooves, only visible in maps generated by the quadratic seismic amplitude, can be traced for shorter distances all over the seabed (Fig. 7c, 13). These grooves have incision depths of <10 m and are 50-200 m wide. The density of this type of curvilinear grooves is constant over the cube, but their spatial arrangement varies: While they are chaotically oriented in water depths of 430-440 m, they mostly follow pre-existing MSGLs in deeper waters (Fig. 7c). The troughs of these grooves are often intersected by transverse ridges and several smaller grooves (Fig. 14).

Interpretation: These variably-oriented curvilinear grooves are interpreted to be iceberg ploughmarks, formed by sediment ploughing by keels of drifting icebergs (Dowdeswell et al., 2008). Their orientation is affected by variations in wind directions, marine currents and seabed topography (Rafaelsen et al., 2002). Their V- to U-shaped morphology with multiple grooves indicates very sharp incision of single- and multi-keel icebergs (Barnes and Lien, 1987; Andreassen et al., 2008). The high rims at the terminus of some of the ploughmarks are, by comparison with similar features farther north in Bjørnøyrenna (Andreassen et al. 2014), interpreted to be iceberg pits or iceberg plough ridges.

Iceberg ploughmarks can be followed over large distances all over the seabed, building the highest rims in areas dominated by thick Quaternary sediments (Fig. 9). We suggest increased variance values at locations characterized by iceberg rimming to indicate sediment reworking (Fig. 12).

Different groups of iceberg ploughmarks can be identified: The first group of icebergs was identified using seismic attribute maps (structure, curvature, dip and variance) (Figs. 9, 12). This group chaotically ploughed in all water depths, thereby not following any pre-existing structures. The group builds rims and becomes gradually deeper towards the terminus (Fig. 9). Some of the ploughmarks of this group end with a terminal berm, indicating places where the iceberg has come to a halt (Lewis et al., 2016), and potentially started to rotate (Woodworth-Lynas et al., 1991; Syvitski et al., 2001) (Fig. 12).

The second group of iceberg ploughmarks was identified in quadratic amplitude maps (Fig. 13) and indicates keels of thinner icebergs. We observe chaotically-oriented iceberg ploughing in shallower water and ploughmarks following pre-existing MSGLs in deeper water depths. Several smaller grooves within these ploughmarks were probably formed by multiple iceberg keels. Due to geometrical and stratigraphical relationships (Fig. 13c), we suggest that a first assemblage of many small ploughmarks eroded the seabed, followed by ploughing of few megabergs.

Corrugation ridges

Description: Regular sets of ~1 m-high parallel transverse ridges occur within some of the grooves of the smaller iceberg ploughmarks (Figs. 14, 15a). These transverse ridges have mean wave lengths of 70 m and are oriented ~perpendicularly to the groove orientation. From their regular shape, these ridges may at first be taken to be processing or acoustic artefacts. However, acoustic artefacts should have imprints parallel to the acquisition direction and in spacing of ~6 m. Due to their systematic wave length of 70 m and orientation transverse to the groove orientation, these features cannot be related to data acquisition.

Interpretation: Based on comparisons with similar features observed in Pine Island Bay, Western Antarctica (Jakobsson et al., 2011), and the northern Barents Sea (Andreassen et al., 2014;

Bjarnadóttir et al., 2014), we interpret these small ridges to be corrugated ridges. The formation of corrugation ridges with extreme regularity in Pine Island Bay, characterized by ~0.5 m high corrugations with a crest spacing of 35-70 m, has been related to the tidal effect of iceberg ploughing (Jakobsson et al., 2011). During low tides, icebergs are expected to squeeze sediment and form transverse ridges (Jakobsson et al., 2011). The tidal range on islands that border the northern Barents Sea is <2 m (www.kartverket.no), thereby supporting that these features are not processing or acoustic artefacts. The spacing of the ridges implies 70 m of ice movement per day, which is rather fast for a grounding line retreat (Amundson et al., 2010).

Pockmarks

Description: A crater-like feature, ~400 m in diameter and ~30 m in depth, is identified in the northwestern part of the study area (Fig. 15). This circular depression is characterized by a ~30° dipping flank and a 14 m high sediment rim. The feature, cutting 8 meters deep into the buried ridge-shaped reflection, appears right above an iceberg groove on URU and a fault terminating in the deeper stratigraphy.

A group of 90-120 m wide and 3-5 m deep circular depressions appear in the southeastern part of the seismic cube (Fig. 16a), where the Quaternary sediment package is thickest. This group of depressions is distributed above some anomalies 15-20 m below URU (Fig. 16b).

Interpretation: Rounded to oval-shaped seabed depressions up to 100 m in diameter and few meters in depth are often related to subsurface fluid-flow (King and MacLean, 1970). Following the interpretations of Solheim and Elverhøi (1985), we suggest these circular depressions to represent pockmarks. The phase-reversed high-amplitude reflections 15-20 m below URU (e.g. Fig. 16b) are likely seismic reflections from sedimentary bedrock layers with gas in the pore space. These layers could act as a fluid source for the seabed pockmarks.

Compared to other areas of the SW Barents Sea (Chand et al., 2016), the seabed in the Hoop area is not densely perforated by pockmarks. Pockmarks are interpreted to have formed where soft-sediment packages were thin enough to allow the fluids escape through the seabed (Solheim and Elverhøi, 1985;

Chand et al., 2016). The up to 65 m thick Quaternary sediment package could therefore act as a seal, only allowing episodic fluid flow. The fluid escape events, however, could have been more explosive, as the dimensions are larger than most of the pockmarks observed in the Barents Sea.

The large semi-circular depression in the center of the study area (Fig. 15) could alternatively be interpreted as an iceberg pit or a crescentic ridge, produced by iceberg instability during rotation or overturn events (compare Stewart et al., 2016; King et al., 2016). However, as it is rimmed against the iceberg drift direction, we speculate about another cause for the feature. The circular imprint along the sub-bottom reflection and its location just above a Jurassic fault (Fig. 15) suggest fluid flow-related processes as a more likely explanation. Since the depression has a 14 m-high rim and a diameter of ~400 m, we suggest that this circular depression was caused by an explosive event related to fluid escape. Individual large pockmarks have also been observed in other areas of the Barents Sea (e.g. Solheim and Elverhøi, 1993; Andreassen et al., 2017).

6. Interpretation of ridge-shaped structure

We interpret the ridge-shaped structure deposited on top of URU as an ice-stream shear margin moraine, formed in the shear zone between a fast-flowing ice-stream and the slow-moving ice-sheet (Stokes and Clark, 2002; Batchelor and Dowdeswell, 2016). The shear margin moraine indicates abrupt changes in ice velocity, with fast-streaming ice to the northwest and slowly-moving ice to the southeast. Different ice-stream flow-sets along the seabed and URU reveal an orientation parallel to the position of the shear margin moraine (Piasecka et al., 2016), and some of them are unilaterally bounded by the moraine. Such ice-flow imprints indicate that similar paleo-ice-stream configurations might have formed this structure. Based on sediment core datings from the Barents Sea (Salvigsen, 1981; Rüther et al., 2011; Kaparulina et al., 2017), we suggest that this shear margin moraine formed during an episode of the Bjørnøyrenna Ice Stream readvance between 16.9 and 15.5 cal. yrs BP.

Shear margin moraines on Stokerson Peninsula in Antarctica are around 500 m wide and 10-50 m high (Stokes and Clark, 2002), a magnitude lower than the Bjørnøyrenna shear margin moraine. As the 3D cube is spatially limited, the extent of the moraine remains uncertain.

The steeply-inclined reflections within the moraine (Fig. 10) are interpreted as shear bands, indicating south-eastwards aggradation of the shear margin moraine. The acoustically chaotic wedges onlapping the shear bands on the steeper side of the moraine (Fig. 10c) are interpreted as mass transport deposits and indicate that the lateral aggradation of the shear margin moraine is accompanied by repeated slope failure. These mass transport deposits have previously been discussed to have an impact on fluid migration and the presence of shallow gas along URU (Bellwald and Planke, in print).

The upper boundary of the moraine is dominated by parallel to sub-parallel sets of iceberg ploughmarks (Fig. 10), similar in width to those identified at the seabed, but significantly deeper. Differences in the same glacio-erosive features on different paleo-surfaces have also been observed in the central North Sea (Dowdeswell and Ottesen, 2013). The stratigraphic location of the shear margin moraine, atop URU and incised by semi-linear iceberg ploughmarks and two sets of MSGLs, could indicate that the Bjørnøyrenna has been affected by more glacier oscillations than previously identified based on only two surfaces. However, the glacio-erosive imprints on the moraine could also be associated with one or multiple ice-streaming phases documented in previous studies (Bjarnadóttir et al., 2014; Piasecka et al., 2016). Landforms of multiple subsequent glacial events on the moraine and the seabed indicate that the ice-stream readvances did not entirely erode the intraglacial sediment package (Fig. 8).

The 3D high-resolution seismic data further indicate a spatial link between the location of the shear margin moraine and a NE-SW oriented topographic high on URU (Fig. 6c), which could have acted as a pinning point for the moraine deposition. Topographic highs have been suggested to provide a stabilizing pinning point for other glacial deposits, such as grounding-zone wedges (Dowdeswell and Fugelli, 2012).

7. Discussion

7.1 Link of seabed expressions with underlying geology

Most of the seabed in the study area is highly affected by glacial erosion (Fig. 7). Besides imprints of paleo-ice-streams, the geomorphology of the contemporary seabed could also be influenced by underlying glacial deposits. Acoustically transparent glacial sediments at the outer Bjørnøyrenna and within Marguerite Trough on the Antarctic Peninsula continental shelf have been interpreted as glacial till (Sættem et al., 1992; Ó Cofaigh et al., 2002). We follow these interpretations and suggest the glacial sediment package of the Hoop area to be dominated by muddy glacial till.

The most elongated and clearly defined MSGLs below the ice stream in the outer Marguerite Bay are developed where a deforming till layer, characterized by low shear strength, is thickest (Dowdeswell et al., 2004). In our study we also observe that the MSGLs occur where the Quaternary sediment package is thickest, which correlates with low-amplitude to transparent reflection patterns below seabed Zone I (Fig. 8c). The P-Cable seismic data indicate subglacial deformation associated with the MSGLs formation to have occurred at least to a depth defined by the height of the lineations. The MSGLs in Zone II, by contrast, are wider and shallower than in Zone I, which could be related to a thinner till layer atop the moraine and sediment reworking by iceberg ploughing.

Taking into account a lower sea level at that time, the icebergs ploughing the contemporary seabed may have been about 400 m high. In previous studies of the region, iceberg ploughing has been reported to be most frequent in water depths from ~400 to 450 m (Piasecka et al., 2016). However, besides having a link with the water depth, the type of iceberg ploughing could also depend on the nature of the underlying strata. Iceberg ploughmarks frequently occur in Zone II, in the area of the buried shear margin moraine (Fig. 6) and the thinnest package of glacial till. Lower subglacial roughness values are modeled for the deepest points of Bjørnøyrenna, while higher subglacial roughness values are modeled towards the flanks and topographic highs (Gudlaugsson et al., 2013). Similar to the results of the subglacial roughness modeling, the moraine could act as a structure contrasting in roughness. Wider and shallower MSGLs and the absence of corrugation ridges in Zone II could thus be explained by roughness contrasts related to the moraine and a higher shear strength

related to the thickness of the Quaternary sediment package. The poor preservation of MSGLs in this area (Fig. 8) is probably related to iceberg scouring and iceberg-related sediment reworking. Multiple sets of ploughmarks could indicate sediment redistribution from existing ridges, and preferential sediment redistribution into depressions afterwards (e.g. infilled and ending MSGLs in Zone II, Fig. 9a).

The western boundary of the smooth seabed characterizing Zone III correlates with the eastern extension of the shear margin moraine (Figs. 6b, 7a). As MSGLs are missing in this area, we suggest Zone III to be covered by slow-moving ice during the last ice-streaming phase in the region. Similar ice stream configurations may have existed at the time the shear margin moraine formed. The pockmarks identified in Zone III are not well preserved, and have probably been degraded over time. We suggest that pockmarks are best identifiable here due to the smooth morphology and a lower degree of glacial erosion. Ice streaming in Zone I and the deposition of the shear margin moraine in Zone II could have acted unfavorably for fluid flow, which might have been most active in areas least affected by ice streams (Zone III). The large pockmark at the Zone I/Zone II boundary may indicate that the moraine acted as a seal for fluid flow (Fig. 15). However, when a critical point of overpressure had been reached, fluids might rapidly have propagated to the seabed, forming this large crater.

Single-keel iceberg ploughmarks of Zone III show wider erosive traces and up to 3 m-high rims (Fig. 16). Therefore we suggest icebergs to have a higher erosional power when underlain by a thick package of low-amplitude to transparent reflections (Fig. 16b). The gravity cores collected from Zone III are longer (2 m in average) compared to gravity cores collected from Zone I and II (1.3 and 1.6 m in average). A higher penetration might indicate softer sediments in Zone III, which were less resistant for upcoming iceberg ploughing.

7.2 Glacial history

The assemblage of different subglacial features preserved in the uppermost 65 m of the sediment package of the Hoop area records the dynamic advance and retreat history of the fast-flowing Barents Sea Ice Stream (BSIS).

Different sets of MSGLs on URU document time periods with streaming grounded ice (Piasecka et al., 2016). Various E-W to NNE-SSW-oriented glacio-erosive features on URU of the P-Cable data concur with these interpretations (Figs. 6c, 17a). Glaciotectonic activity related to these glaciations probably resulted in the deformed strata below URU (Fig. 4). A shear margin moraine has been formed during the last glaciation along URU, indicating ice streaming northwest of it and slowly moving ice to the southeast. Shear heating and heavily crevassed ice at the lateral boundary of the ice stream most likely gave accommodation space for the build-up of the moraine. Correlating with a topographic high along URU, the moraine was affected by repeated slope failures (Fig. 17a) (Bellwald and Planke, in print).

The occurrence of MSGLs and wider buried iceberg ploughmarks on the top of the shear margin moraine indicates the presence of a fast-flowing ice stream and drifting icebergs that grounded and ploughed the moraine. The ploughing occurred probably due to the disintegration of the BSIS that formed the MSGLs at the top of the moraine (Fig. 17b). Afterwards, an up to 65 m-thick sediment package has been deposited atop URU and the moraine (Fig. 17c). This sediment package, most likely consisting of glacial till overlain by a thin (glaci)marine layer (Sættem et al., 1992), flattened the pre-existing glacial topography.

Different sets of MSGLs along the seabed record different ice streaming events of the BSIS in the central and western part of the cube (Fig. 17d). However, the BSIS did erode neither into the moraine nor URU during the streaming phases indicated on the seabed. During the disintegration of the BSIS, the seabed has been heavily ploughed by the keels of drifting icebergs. Two groups of icebergs subsequently traversed and reworked existing subglacial landforms during deglaciation periods, producing distinctive sets of ploughmarks. The second-order iceberg ploughmarks, characterized by a low degree of erosion and rimming (Figs. 7c and 13), are suggested to represent a spatially extensive ice disintegration into numerous small icebergs during a rapid ice stream collapse (Fig. 17e). This chaotic mélange of icebergs could be an analogue of what is currently observed in glacier tongues in Porpoise Bay in Antarctica (Miles et al., 2017). The first-order iceberg ploughmarks, which can be followed for several kilometers and occasionally build up meter-high rims (Fig. 7b), are suggested to

represent the normal iceberg assemblage related to the collapse of the BSIS (Fig. 17f). Calving icebergs of this first-order group cut into the smaller iceberg ploughmarks. Icebergs forming the first-order ploughmarks are suggested to represent a rather discrete detachment of large icebergs ("megabergs") that likely calved from the grounded edge of the rapidly-flowing glacial margin. As ploughmarks and MSGLs expressed on the contemporary seabed do not cut into the shear margin moraine (Figs. 8, 9), the moraine seems to have acted as the glacio-erosive limit for landforms identified at the seabed.

8. Conclusions

High-resolution P-Cable 3D seismic data are a very useful tool for imaging the details of glacial landforms and studying the link between the seabed morphology and the underlying geology in the SW Barents Sea, providing new insights about the configuration, dynamics and retreat pattern of the Barents Sea Ice Stream. Combining small-scale observations with new large-scale glacial landforms, a revised model for Barents Sea Ice Stream dynamics of the Hoop area is presented in this study.

The use of seismic attributes allows to distinguish different types of iceberg ploughmarks and evaluate the effect of tides and currents on the pathway of icebergs. Small-scale iceberg ploughmarks and corrugation ridges illustrate that the P-Cable technology can image and characterize glacial deposits on a meter-scale. Comparisons with seabed images generated by conventional multi-beam echosounder data and conventional 3D seismic data show that the P-Cable technology resolves the seabed in a similar to higher quality. Buried glacial horizons, such as the top of a shear margin moraine and Upper Regional Unconformity, can be mapped at MBE-quality using the P-Cable technology.

Seismic imaging of large buried glacial landforms has been successfully carried out, using the example of a shear margin moraine with glacio-erosive features at its top. Based on seismic geomorphology, we suggest ice-streaming in the northwest and more slowly moving ice southeast of the moraine. Buried iceberg ploughmarks and mega-scale glacial lineations at the top of this moraine

indicate possibly more ice streaming events than previously interpreted from conventional seismic data.

The P-Cable data indicate a strong link between glacial geomorphic features on the contemporary seabed and the underlying geology. A combination of paleo-ice stream dynamics as well as glacial structures identified within the Quaternary sediment package is suggested to cause the geomorphology of the seabed. Evidence of catastrophic fluid expulsions and the sealing by glacial sediments is suggested from a 400 m wide pockmark located where the moraine thins out.

Acknowledgements

We thank Colm O'Cofaigh, Chris Stokes, Monica Winsborrow and Stéphane Polteau for thorough discussions and constructive feedback. TGS, WGP and VBPR are acknowledged for data availability. Nina Lebedeva-Ivanova and Dwarica Maharjan are acknowledged for help with the bathymetric data and the data base. The research leading to these results has received funding from the People Programme (Marie Curie Actions) of the European Union's Seventh Framework Programme FP7/2007-2013/ under REA grant agreement n° 317217. The research forms part of the GLANAM (GLAciated North Atlantic Margins) Initial Training Network. We further acknowledge the support from the Research Council of Norway through its Centres of Excellence funding scheme, project 22372.

References

Amundson, J.M., Fahnestock, M., Truffer, M., Brown, J., Lüthi, M.P., 2010. Ice mélange dynamics and implications for terminus stability, Jakobshavn Isbræ, Greenland. Journal of Geophysical Research 115, F01005.

Andreassen, K., Ødegaard, C.M., Rafaelsen, B., 2007. Imprints of former ice streams, imaged and interpreted using industry three-dimensional seismic data from the south-western Barents Sea. Geological Society, London, Special Publications 277, 151-169.

Andreassen, K., Laberg, J.S., Vorren, T.O., 2008. Seafloor geomorphology of the SW Barents Sea and its glaci-dynamic implications. Geomorphology 97, 157-177.

Andreassen, K., Winsborrow, M., 2009. Signature of ice streaming in Bjørnøyrenna, Polar North Atlantic, through the Pleistocene and implications for ice-stream dynamics. Annals of Glaciology 50, 17-26.

Andreassen, K., Winsborrow, M.C.M., Bjarnadóttir, L.R., Rüther, D.C., 2014. Ice stream retreat dynamics inferred from an assemblage of landforms in the northern Barents Sea. Quaternary Science Reviews 92, 246-257.

Andreassen, K., Hubbard, A., Winsborrow, M., Patton, H., Vadakkepuliyambatta, S., Plaza-Faverola, A., Gudlaugsson, E., Serov, P., Deryabin, A., Mattingsdal, R., Mienert, J., Bünz, S., 2017. Massive blow-out craters formed by hydrate-controlled methane expulsion from the Arctic seafloor. Science, 356, 948-953.

Barnes, P.W., Lien, R., 1987. Icebergs rework shelf sediment to 500 m off Antarctica. Geology 16, 1130-1133.

Batchelor, C.L., Dowdeswell, J.A., 2016. Lateral shear-moraines and lateral marginal-moraines of palaeo-ice streams. Quaternary Science Reviews 151, 1-26.

Bellwald, B., Hjelstuen, B.O., Sejrup, H.P., Haflidason, H., 2016. Postglacial Mass Movements and Depositional Environments in a High-Latitude Fjord System – Hardangerfjorden, Western Norway. Marine Geology 379, 157-175.

Bellwald, B., Planke, S., in print. Shear margin moraine, mass transport deposits, and soft beds revealed by high-resolution P-Cable 3D seismic data in the Hoop Area, Barents Sea. Special publication, Geological Society of London.

Bjarnadóttir, L.R., Rüther, D.C., Winsborrow, M.C.M., Andreassen, K., 2013. Grounding-line dynamics during the last deglaciation of Kveithola, W Barents Sea, as revealed by seabed geomorphology and shallow seismic stratigraphy. Boreas 42, 84-107.

Bjarnadóttir, L.R., Winsborrow, M.C.M., Andreassen, K., 2014. Deglaciation of the central Barents Sea. Quaternary Science Reviews 92, 208-226.

Brown, A.R., 1999. Interpretation of three-dimensional seismic data. 5th edition. AAPG Memoir 42, Tulsa, Oklahoma, 514 pp.

Chand, S., Thorsnes, T., Rise, L., Brunstad, H., Stoddart, D., 2016. Pockmarks in the SW Barents Sea and their links with iceberg ploughmarks. In: Dowdeswell, J. et al. (Eds.), Atlas of submarine glacial landforms: Modern, Quaternary and Ancient. Geological Society, London, Memoirs, 46, 281-282.

Clark, C.D., 1993. Mega-scale glacial lineations and cross-cutting ice-flow landforms. Earth Surface Processes and Landforms 18, 1-29.

Clark, C.D., Tulaczyk, S.M., Stokes, C.R., Canals, M., 2003. A groove-ploughing theory for the production of mega-scale glacial lineations and implications for ice-stream mechanics. Journal of Glaciology 49, 240-256.

Crutchley, G.J., Karstens, J., Berndt, C., Talling, P.J., Watt, S.F.L., Vardy, M.E., Hühnerbach, V., Urlaub, M., Sarkar, S., Klaeschen, D., Paulatto, M., Le Friant, A., Lebas, E., Maeno, F., 2012. Insights into the emplacement dynamics of volcanic landslides from high-resolution 3D seismic data acquired offshore Montserrat, Lesser Antilles. Marine Geology 335, 1-15.

Dowdeswell, J.A., Ó Cofaigh, C., Pudsey, C.J., 2004. Thickness and extent of the subglacial till layer beneath an Antarctic paleo-ice stream. Geology 32, 13-16.

Dowdeswell, J.A., Ottesen, D., Evans, J., Ó Cofaigh, C., Anderson, J.B., 2008. Submarine glacial landforms and rates of ice-stream collapse. Geology 36, 819-822.

Dowdeswell, J.A., Hogan, K.A., Evans, J., Noormets, R., Cofaigh, C.O., Ottesen, D., 2010. Past ice-sheet flow east of Svalbard inferred from streamlined subglacial landforms. Geology 38, 163-166.

Dowdeswell, J.A., Fugelli, E.M.G., 2012. The seismic architecture and geometry of grounding-zone wedges formed at the marine margins of past ice sheets. GSA Bulletin 124, 1750-1761.

Dowdeswell, J.A., Ottesen, D., 2013. Buried iceberg ploughmarks in the early Quaternary sediments of the central North Sea: A two-million year record of glacial influence from 3D seismic data. Marine Geology 344, 1-9.

Dowdeswell, J.A., Ottesen, D., 2016. Three-dimensional seismic imagery of deeply buried iceberg ploughmarks in North Sea sediments. In: Dowdeswell, J. et al. (Eds.), Atlas of submarine glacial landforms: Modern, Quaternary and Ancient. Geological Society, London, Memoirs, 46, 281-282.

Elverhøi, A., Solheim, A., 1984. Barents Sea ice sheet – a sedimentological discussion. Polar Research 1, 23-42.

Faleide, J.I., Solheim, A., Fiedler, A., Hjelstuen, B.O., Andersen, E.S., Vanneste, K., 1996. Late Cenozoic evolution of the Barents Sea-Svalbard continental margin. Global and Planetary Change 12, 53-74.

Fiedler, A., Faleide, J.I., 1996. Cenozoic sedimentation along the southwestern Barents Sea margin in relation to uplift and erosion of the shelf. Global and Planetary Change 12, 75-93.

Forman, S., 2004. A review of postglacial emergence on Svalbard, Franz Josef Land and Novaya Zemlya, northern Eurasia. Quaternary Science Reviews 23, 1391-1434.

Gudlaugsson, E., Humbert, A., Winsborrow, M., Andreassen, K., 2013. Subglacial roughness of the former Barents Sea ice sheet. Journal of Geophysical Research, Earth Surface, 118, 2546-2556.

Henriksen, E., Ryseth, A.E., Larssen, G.B., Heide, T., Rønning, K., Sollid, K., Stoupakova, A.V., 2011. Tectonostratigraphy of the greater Barents Sea: implications for petroleum systems. In: Spencer, A.M. et al. (Eds.), Arctic Petroleum Geology. Geological Society, London, Memoirs, 35, 163-195.

Hustoft, S., Bünz, S., Mienert, J., Chand, S., 2009. Gas hydrate reservoir and active methane-venting province in sediments on <20 Ma young oceanic crust in the Fram Strait, offshore NW-Svalbard. Earth and Planetary Science Letters 284, 12-24.

Jakobsson, M., Anderson, J.B., Nitsche, F.O., Dowdeswell, J.A., Gyllencreutz, Kirchner, N., Mohammad, R., O'Regan, M., Alley, R.B., Anandakrishnan, S., Eriksson, B., Kirshner, A., Fernandez, R., Stolldorf, T., Minzoni, R., Majewski, W., 2011. Geological record of ice shelf break-up and grounding line retreat, Pine Island Bay, West Antarctica. Geology 39, 691-694.

Jakobsson, M., Mayer, L., Coakley, B., Dowdeswell, J.A., Forbes, S., Fridman, B., Hodnesdal, H., Noormets, R., Pedersen, R., Rebesco, M., Schenke, H.W., Zarayskaya, Y., Accettella, D., Armstrong, A., Anderson, R.M., Bienhoff, P., Camerlenghi, A., Church, I., Edwards, M., Gardner, J.V., Hall, J.K., Hell, B., Hestvik, O., Kristoffersen, Y., Marcussen, C., Mohammad, R., Mosher, D., Nghiem, S.V., Pedrosa, M.T., Travaglini, P.G., Weatherall, P., 2012. The International Bathymetric Chart of the Arctic Ocean (IBCAO) Version 3.0. Geophysical Research Letters 39, 12609.

Jakobsson, M., Gyllencreutz, R., Mayer, L.A., Dowdeswell, J.A., Canals, M., Todd, B.J., Dowdeswell, E.K., Hogan, K.A., Larter, R.D., 2016. Mapping submarine glacial landforms using acoustic methods. In: Dowdeswell, J. et al. (Eds.), Atlas of submarine glacial landforms: Modern, Quaternary and Ancient. Geological Society, London, Memoirs, 46, 17-40.

Kallweit, R.S., Wood, L.C., 1982. The limits of resolution of zero-phase wavelets. Geophysics 47, 135-1046.

Kaparulina, E., Junttila, J., Strand, K., Lunkka, J.P., 2017. Provenance signatures and changes of the southwestern sector of the Barents Ice Sheet during the last deglaciation. Boreas 12293.

Karstens, J., Crutchley, G.J., Berndt, C., Talling, P.J., Watt, S.F.L., Hühnerbach, V., Le Friant, A., Lebas, E., Trofimovs, J., 2013. Emplacement of pyroclastic deposits offshore Montserrat: Insights from 3D seismic data. Journal of Volcanology and geothermal Research 257. 1-11.

King, L.H., MacLean, B., 1970. Pockmarks on the Scotian shelf. Geological Society of America Bulletin 81, 3141-3148.

King, E.L., Rise, L., Bellec, V.K., 2016. Crescentic submarine hills and holes produced by iceberg calving and rotation. In: Dowdeswell, J. et al. (Eds.), Atlas of submarine glacial landforms: Modern, Quaternary and Ancient. Geological Society, London, Memoirs, 46, 267-268.

Kjemperud, A., Fjeldskaar, W., 1992. Pleistocene glacial isostasy – implications for petroleum geology, in: Larsen, R.M.H. et al. (Eds.), Structural and Tectonic Modelling and its Application to Petroleum Geology, NPF Special Publication 1, 187-195.

Laberg, J.S., Andreassen, K., Vorren, T.O., 2012. Late Cenozoic erosion of the high-latitude southwestern Barents Sea shelf revisited. Geological Society of America Bulletin 124, 77-88.

Landvik, J., Bondvik, S., Elverhøi, A., Fjeldskaar, W., Mangerud, J., Salvigsen, O., Siegert, M., Svendsen, J.I., Vorren, T.O., 1998. The last glacial maximum of Svalbard and the Barents Sea area: ice sheet extent and configuration. Quaternary Science Reviews 17, 43-75.

Leenhart, O., 1972. Le sondage sismique continu. Masson and Cie, Paris.

Lewis, C.F.M., Todd, B.J., Sonnichsen, G.V., King, T., 2016. Iceberg-seabed interaction on northwestern Makkovik Bank, Labrador Shelf, Canada. In: Dowdeswell, J. et al. (Eds.), Atlas of submarine glacial landforms: Modern, Quaternary and Ancient. Geological Society, London, Memoirs, 46, 279-280.

Miles, B.W.J., Stokes, C.R., Jamieson, S.S.R., 2017. Simultaneous disintegration of outlet glaciers in Porpoise Bay (Wilkes Land), East Antarctica, driven by sea ice break-up. The Cryosphere 11, 427-442.

Nishenko, S., Hogan, P., Kvitek, R., 2012. Seafloor Mapping for Earthquake, Tsunami Hazard Assessments. Sea Technology 703, 4 pp.

Ottesen, D., Rise, L., Knies, J., Olsen, L., Henriksen, S., 2005. The Vestfjorden-Trænadjupet palaeo-ice stream drainage system, mid-Norwegian continental shelf. Marine Geology 218, 175-189.

Ó Cofaigh, C., Pudsey, C.J., Dowdeswell, J.A., Morris, P., 2002. Evolution of subglacial bedforms along a paleo-ice stream, Antarctic Peninsula continental shelf. Geophysical Research Letters 29 (8).

Ó Cofaigh, C., Dowdeswell, J.A., Allen, C.S., Hiemstra, J.F., Pudsey, C.J., Evans, J., Evans, D.J.A., 2005. Flow dynamics and till genesis associated with a marine-based Antarctic paleo-ice stream. Quaternary Science Reviews 24, 709-740.

Ó Cofaigh, C., Stokes, C.R., 2008. Reconstructing ice-sheet dynamics from subglacial sediments and landforms: introduction and overview. Earth Surface Processes and Landforms 33, 495-502.

Patton, H., Hubbard, A.L., Andreassen, K., Winsborrow, M., Stroeven, A.P., 2016. The build-up, configuration, and dynamical sensitivity of the Eurasian ice-sheet complex to Late Weichselian climatic and oceanic forcing. Quaternary Science Reviews 153, 97-121.

Piasecka, E.D., Winsborrow, M.C.M., Andreassen, K., Stokes, C.R., 2016. Reconstructing the retreat dynamics of the Bjørnøyrenna Ice Stream based on new 3D seismic data from the central Barents Sea. Quaternary Science Reviews 151, 212-227.

Planke, S., Eriksen, F.N., Berndt, C., Mienert, J., Masson, D.G., 2009. P-Cable high-resolution seismic. Oceanography 22, 85.

Plaza-Faverola, A., Bünz, S., Mienert, J., 2011. Repeated fluid expulsion through sub-seabed chimneys offshore Norway in response to glacial cycles. Earth and Planetary Science Letters 305, 297-308.

Posamentier, H.W., Davies, R.J., Cartwright, J.A., Wood, L., 2007. Seismic geomorphology – an overview. Geological Society, London, Special Publications, 277, 1-14.

Rafaelsen, B., Andreassen, K., Kuilman, L.W., Lebesbye, E., Hogstad, K., Midtbø, M., 2002. Geomorphology of buried glacigenic horizons in the Barents Sea from three-dimensional seismic data. In: Dowdeswell, J.A. and Ó Cofaigh, C., (eds). Glacier-Influenced Sedimentation on High-Latitude Continental Margins. Geological Society, London, Special Publications, 203, 259-276.

Rüther, D.C., Mattingsdal, R., Andreassen, K., Forwick, M., Husum, K., 2011. Seismic architecture and sedimentology of a major grounding zone system deposited by the Bjørnøyrenna Ice Stream during Later Weichselian deglaciation. Quaternary Science Reviews 30, 2776-2792.

Rüther, D.C., Winsborrow, M., Andreassen, K., Forwick, M., 2017. Grounding line proximal sediment characteristics at a marine-based late-stage ice stream margin. Journal of Quaternary Science 32 (4), 463-474.

Salvigsen, O., 1981. Radiocarbon dated raised beaches in Kong Karls Land, Svalbard, and their consequences for the glacial history of the Barents Sea. Geografiska Annaler 63, 280-291.

Shaw, J., Piper, D.J.W., Fader, G.B.J., King, E.L., Todd, B.J., Bell, T., Batterson, M.J., Liverman, D.G.E., 2006. A conceptual model of deglaciation of Atlantic Canada. Quaternary Science Reviews 25, 2059-2081.

Sheriff, R.E., 1997. Encyclopedic Dictionary of Exploration Geophysics. Societey of Exploration Geophysicists. Third edition. 386 pp.

Siegert, M.J., Dowdeswell, J.A., 1996. Spatial variations in heat at the base of the Antarctic ice sheet from analysis of the thermal regime above subglacial lakes. Journal of Glaciology 42, 501-509.

Sigmond, E.M.O., 1992. Berggrunnskart, Norge med havområder. Målestokk 1:3 millioner. Norges geologiske undersøkelse.

Solheim, A., Kristoffersen, Y., 1984. Sediment Distribution Above the Upper Regional Unconformity and the Glacial History of Western Barents Sea. Norsk Polarinstitutt Skrifter. 189 (B).

Solheim, A., Elverhøi, A., 1985. A pockmark field in the Central Barents Sea; gas from a petrogenic source? Polar Research 3, 11-19.

Solheim, A., Elverhøi, A., 1993. Gas-related sea floor craters in the Barents Sea. Geo-Marine Letters 13, 235-243.

Solheim, A., Andersen, E.S., Elverhøi, A., Fiedler, A., 1996. Late Cenozoic depositional history of the western Svalbard continental shelf, controlled by subsidence and climate. Global and Planetary Change 12, 135-148.

Stokes, C.R., Clark, C.D., 2002. Ice stream shear margin moraines. Earth Surface Processes and Landforms 27, 547-558.

Svendsen, J.I., Gataullin, V., Mangerud, J., Polyak, L., 2004. The glacial History of the Barents and Kara Sea Region, in: Ehlers, J., Gibbard, P.L. (Eds.), Developments in Quaternary Sciences. Elsevier, 369-378.

Syvitski, J.P.M., Stein, A.B., Andrews, J.T., Milliman, J.D., 2001. Icebergergs and the sea floor of the East Greenland (Kangerlussuaq) continental margin. Arctic, Antarctic and Alpine Research 33, 52-61.

Sættem, J., Poole, D.A.R., Ellingsen, L., Sejrup, H.P., 1992. Glacial geology of outer Bjørnøyrenna, southwestern Barents Sea. Marine Geology 103, 15-51.

Sættem, J., Bugge, T., Fanavoll, S., Goll, R.M., Mørk, A., Mørk, M.B.E., Smelror, M., Verdenius, J.G., 1994. Cenozoic margin development and erosion of the Barents Sea: Core evidence from southwest of Bjørnøya. Marine Geology 118, 257-281.

Stewart, T.J., Stagpoole, V.M., Woode, R.A., Carter, L., 2016. Ploughmarks and pits on the Chatham Rise: a record of deep-keeled Antarctic icebergs at 43˚ 20' S. In: Dowdeswell, J. et al. (Eds.), Atlas of submarine glacial landforms: Modern, Quaternary and Ancient. Geological Society, London, Memoirs, 46, 281-282.

Trabant, P.K., 1984. Applied High-Resolution Geophysical Methods. Boston, Ma., International Human Resources Development Corporation, p. 103.

Tulaczyk, S., Scherer, R., Clark, CD., 2001. A ploughing model for the origin of weak tills beneath ice streams: a qualitative statement. Quaternary International 86, 59-70.

Vadakkepuliyambatta, S., Bünz, S., Tasianas, A., Mienert, J., 2016. Iceberg ploughmarks in the SW Barents Sea imaged using high-resolution P-Cable 3D seiscmi data. In: Dowdeswell, J. et al. (Eds.), Atlas of submarine glacial landforms: Modern, Quaternary and Ancient. Geological Society, London, Memoirs, 46, 281-282.

Vorren, T.O., Kristoffersen, Y., Andreassen, K., 1986. Geology of the inner shelf west of North Cape, Norway. Norsk Geologisk Tidsskrift 66, 99-105.

Vorren, T.O., Lebesbye, E., Larsen, K.B., 1990. Geometry and genesis of the glacigenic sediments in the southern Barents Sea. Geological Society, London, Special Publications 53, 269-288.

Vorren, T.O., Richardsen, G., Knutsen, S.M., Henriksen, E., 1991. Cenozoic erosion and sedimentation in the western Barents Sea. Marine and Petroleum Geology 8, 317-340.

Vorren, T.O., Rokoengen, K., Bugge, T., Larsen, O.A., 1992. The Continental Shelf, Thickness of Quaternary Sediments: Nasjonalatlas for Norge, kartblad 2.3.9: Hønefoss, Norway. Statens Kartverk 1.

Vorren, T.O., Laberg, J.S., 1997. Trough Mouth Fans - Palaeoclimate and ice-sheet monitors. Quaternary Science Reviews 16, 865-881.

Vorren, T.O., Laberg, J.S., Blaume, F., Dowdeswell, J.A., Kenyon, N.A., Mienert, J., Rumohr, J., Werner, F., 1998. The Norwegian-Greenland sea continental margins: morphology and late Quaternary sedimentary processes and environment. Quaternary Science Reviews 17, 273-302.

Widmaier, M., O'Dowd, D., Delarue, C., 2017. Strategies for High Resolution Towed Streamer Acquisition and Imaging of Shallow Targets. SEG Technical Program Expanded Abstracts 2017, 186-190.

Winsborrow, M.C.M., Andreassen, K., Corner, C.D., Laberg, J.S., 2010. Deglaciation of a marine-based ice sheet: Late Weichselian palaeo-ice dynamics and retreat in the southern Barents Sea reconstructed from onshore and offshore glacial geomorphology. Quaternary Science Reviews 29, 424-442.

Woodworth-Lynas, C.M.T., Josenhans, H.W., Barrie, J.V., Lewis, C.F.M., Parrott, D.R., 1991. The physical processes of seabed disturbance during iceberg grounding and scouring. Continental Shelf Research 11, 939-961.

www.kartverket.no, The Norwegian Hydrographic Service, Stavanger, Norway, 24.05.2017

www.km.kongsberg.com, Kongsberg Maritime AS, Kongsberg, Norway, 12.04.2017.

www.npd.no, Norwegian Petroleum Directorate (NPD), Stavanger, Norway, 30.09.2016.

www.pcable.com, P-Cable 3D Seismics AS, Oslo, Norway, 31.08.2016.

www.seafloorsystems.com, Seafloor Systems Inc., Shingle Springs, USA, 10.05.2017.

Figure captions

Fig. 1. a) Bathymetric map of the study area with major glacial landforms and ice flow directions. The maximum extension of the Barents Sea Ice Sheet during the Last Glacial Maximum (LGM) is marked as white line (Svendsen et al., 2004). Arrows indicate previously inferred major ice stream directions (Andreassen and Winsborrow, 2009; Bjarnadóttir et al., 2013; Rüther et al., 2013). Deglaciation ages (black dots; Salvigsen, 1981; Rüther et al., 2011), ice margin positions (Winsborrow et al., 2010; Bjarnadóttir et al., 2013; Rüther et al., 2013), ice dome (Dowdeswell et al., 2010), and ice divide (Ottesen et al., 2005) are indicated. TMF: Trough mouth fan. **b)** Study area with locations of NPD exploration wells, P-Cable 3D seismic data, gravity cores, and previously mapped streamlined and curvilinear grooves in conventional 3D seismic data (Piasecka et al., 2016).

Fig. 2. Comparison of vertical resolution of seismic data collected by different technologies in the study area. P-Cable 3D seismic data have a vertical resolution of 1-5 m at the seabed and URU. Conventional seismic data have a vertical resolution of c. 8 m at the seabed and URU. The three reflections interpreted in this study are shown in color. The top moraine reflection is not visible in conventional seismic data. Profile location indicated in Fig. 1b. Data courtesy TGS, WGP, and VBPR.

Fig. 3. Comparison of horizontal resolution of the seabed collected by different technologies in the study area. Map location indicated in Fig. 1b. **a)** Swath of MBE (multibeam echosounder; Reson SeaBat 7111, 100 kHz) overlying the P-Cable 3D seismic surface. Black box indicates focused area of Figs. 3a and 3b. **b)** Structure maps over an individual pockmark. P-Cable 3D seismic data have a bin size of 6.25x4.75 m, and a horizontal resolution of 2-10 m. MBE data have a horizontal resolution of

2-4 m and a beam density of c. 3 m. Conventional 3D seismic data have a bin size of 12.5x18.75 m and a horizontal resolution of c. 16 m. **c)** Slope gradient maps over the same pockmark. Data courtesy TGS, WGP, and VBPR.

Fig. 4. Reflections and sequences of the shallow subsurface in the Hoop area. Picked horizons include seabed as the first positive-amplitude reflection, URU (Upper Regional Unconformity) as the positive-amplitude reflection separating the Quaternary package from the underlying sedimentary rocks, and Top moraine as the positive-amplitude reflection in between URU and seabed. Profile location indicated in Fig. 1b.

Fig. 5. Examples of high-resolution gridding using P-Cable 3D seismic data with a bin size of 6.25x4.75m. **a)** Isopach map of the intraglacial sediment package, which is defined as the sequence between the seabed and Upper Regional Unconformity (URU). The map has been generated by subtracting the structure map of the seabed from the structure map of URU. **b)** Seismic attribute map of the seabed dip angle. MSGL: Mega-scale glacial lineation.

Fig. 6. Surfaces of the picked horizons using a velocity of 1500 m/s for time-to-depth conversion. **a)** Seabed. **b)** Shear margin moraine. In areas where no moraine has been mapped, URU is displayed instead. **c)** URU. Indicated structures include groove sets (white arrows) and the projected location of the large pockmark identified on the seabed (white circle).

Fig. 7. Glacial landforms and zonation of the seabed. **a)** Combined curvature and structure map of the seabed with indicated zone boundaries. **b)** Interpreted major glacial landforms. Most of these expressions are also visible in conventional 3D seismic data. **c)** Interpreted minor glacial landforms. These expressions are not visible in conventional 3D seismic data.

Fig. 8. Expression of the different subglacial landforms and their link to the underlying stratigraphy. **a)** Structure and curvature map of the seabed. Thin white stippled lines indicate pathways of some iceberg ploughmarks. For map location, see Fig. 6a. **b+c)** Seismic profiles focusing on the geometries of subglacial landforms in the different zones. Landforms indicated in red mark streamlined grooves, interpreted as mega-scale glacial lineations (MSGLs). Landforms indicated in white mark curvilinear grooves, interpreted as iceberg ploughmarks. Zone I is dominated by ENE-WSW-oriented flow sets of MSGLs. Iceberg ploughmarks represent the most dominant glacial landform in Zone II, and often cut into the troughs of MSGLs. Note some partly infilled MSGLs in Zone II. Zone III is characterized by an absence of MSGLs, but occasionally eroded by ploughmarks. **d)** Geometries of different landforms. Locations of landforms are indicated in Figs. 8b and 8c.

Fig. 9. Links between iceberg ploughing and underlying geology. **a)** Curvature map showing pathway of one particular iceberg in Zone I and II (red stippled line). **b)** Seismic profiles showing the link between the style of iceberg ploughing and the underlying geology. Both iceberg erosion and rimming

increase in a westward direction, where the intraglacial package is dominated by low-amplitude reflections. Note that the ploughmark indicates an iceberg break-up in Zone I. For map location, see Fig. 6a.

Fig. 10. Buried shear margin moraine and structures related to its formation. **a)** Structure map of Top moraine with major iceberg ploughmarks (indicated by numbers). Geometry of ploughmark 6 in the top right corner. **b)** Seismic profile showing glacio-erosive structures along the top of the shear margin moraine. **c)** Seismic profile showing the internal architecture of the shear margin moraine.

Fig. 11. Iceberg ploughmarks along the shear margin moraine. **a)** Structure map showing NNE-SSW-oriented iceberg ploughmarks along the Top moraine horizon. Note the multi-keel iceberg ploughmark (IPM) in the center of the figure. Location of seismic profile indicated by stippled white line. **b-d)** Visualization of iceberg ploughing along the shear margin moraine using different seismic attributes. **b)** Original seismic amplitude. **c)** Blending of original seismic amplitude and quadratic amplitude. **d)** RMS amplitude. For map location, see Fig. 10a.

Fig. 12. Seismic attribute maps used to better image the glacio-erosive behavior of an iceberg, here expressed as an iceberg pit. **a)** Structure and curvature map across the seismic cube. For map location, see Fig. 6a. **b)** Map of the dip angle as a useful tool to highlight the steeper flanks. White stippled line indicates erosion by the keel of the iceberg. **c)** Variance map as a useful tool to identify areas characterized by reworked sediment. Areas marked by stippled white lines indicate reworked sediment. **d)** Seismic profiles showing that rims and degree of erosion increase along the pathway of the iceberg. Reworked iceberg rims are indicated in pink.

Fig. 13. Types of iceberg ploughmarks. **a)** Structure map showing major iceberg ploughmarks and iceberg pits. These expressions are also visible in conventional 3D seismic data. **b)** Quadratic amplitude map showing minor iceberg ploughmarks (thin white lines). These expressions are not visible in conventional 3D seismic data. **c)** Seismic profile showing the geomorphologic expressions of two minor iceberg ploughmarks (1 and 2) and one major iceberg ploughmark (3). For map location, see Fig. 6a.

Fig. 14. Corrugated ridges identified within the troughs of mega-scale glacial lineations. **a)** 3D view of corrugated ridges and large iceberg ploughmarks. **b)** Seismic profile in a trough of a mega-scale glacial lineation, crosscut twice by (multi-keel) iceberg ploughmarks. Profile location shown in Fig. 14a. **c)** Seismic profile showing expression and frequency of corrugations (crest-to-crest spacing of ~70 m, height of ~1 m) in the seismic data. For map location, see Fig. 6a.

Fig. 15. a) Structure map of the large pockmark, located in an area dominated by mega-scale glacial lineations, occasionally crosscut by iceberg ploughmarks. **b)** Seismic profile of the pockmark and its link with the deeper geology. Note the rim of the landform and the crosscutting of the structure into

the shear margin moraine. Indicated are Cenozoic faults (stippled lines), potential fluid pathways (arrows) and a buried groove along URU. For map location, see Fig. 6a.

Fig. 16. Seabed of Zone III. **a)** Structure map showing flat seabed intersected by pockmarks and iceberg ploughmarks. **b)** Seismic profile showing dimensions of pockmarks and iceberg ploughmarks on the flat seabed. Indicated is also the link between the pockmark field on the seabed and a field characterized by high-amplitude reflections in the deeper stratigraphy. For map location, see Fig. 6a.

Fig. 17. Glacial model of the study area, with ice flowing towards the reader. Note that the geology in the schematic models is vertically exaggerated, and that the dimensions of ice and water are not in relation to the exaggeration of the geology. Images to the right are structure maps of the different surfaces. **a)** Glacio-tectonically deformed strata below URU and glacio-erosive landforms at URU indicate multiple streaming phases of the Barents Sea Ice Stream. The lateral deposition of a shear margin moraine, whose location correlates with a topographic high along URU, indicates different ice stream dynamics (between fast flowing ice stream and slow flow of the ice sheet). Accommodation space and sediment supply for the deposition of the moraine due to shear heat (S) and heavily crevassed ice. Occurrence of repeated submarine slope failure during the formation of the moraine. **b)** Icebergs ploughing into URU and the shear margin moraine after ice-sheet break-up. The iceberg ploughmarks along the moraine are semi-linear. **c)** Deposition of Quaternary sediment package, flattening the pre-existing topography. This package is dominated by glacial till. **d)** Multiple ice-streaming events of the Barents Sea Ice Stream forming different sets of MSGLs along the seabed. The absence of MSGLs in the flat seabed to the east of the cube indicates that slow-flowing ice was dominant in that area. **e)** Ice-sheet break-up and iceberg ploughing along the seabed. Many small, tabular icebergs erode the seabed in a first phase. These icebergs often follow the troughs of the MSGLs, where they form corrugated ridges. Sediment reworking might result in less pronounced MSGLs. Fluid systems are suggested to be active. **f)** Few large icebergs deeply ploughing into grooves of smaller icebergs in a second phase of ice-sheet break-up. Sediment reworking is suggested to infill pre-existing seabed expressions. Fluid systems are suggested to be still active.

Tab. 1. Characterization of seismic reflections and seismic sequences of the shallow subsurface. Reflections and sequences are indicated in Fig. 4.

Tab. 2. Comparison of geophysical techniques currently used in marine studies. Vertical resolution is defined by quarter of a wave length (λ/4). Horizontal resolution is defined by the 1st Fresnel Zone for MBE systems. As seismic data can be migrated, the horizontal resolution of 3D seismic data is defined by λ/4 as well. MBE: Multibeam echosounder; λ: wave length. *Dominant frequency, **Maximum detectable frequency within a reliable seismic range of -20 dB, ***Estimations for observed data.

Table 1

1	**Seabed reflection**	**Strong, positive, continuous**	**Subglacial, iceberg ploughing, fluid escape**
2	URU reflection	Strong, positive, continuous	Subglacial, iceberg ploughing, fluid escape, thermokarst
3	Top moraine reflection	Moderate, positive, discontinuous	Subglacial, iceberg ploughing, slope failure
4	Soft reflection	Strong, negative, discontinuous	Weak bed deposition, gas-charged layer, turbidite
5	Intraglacial package	Weak	Glacial/deglacial deposition
6	Shear margin moraine	Weak	Subglacial sediment accumulation, ice-stream shearing
7	Mass transport deposit reflection	Moderate to weak, positive	Slope failure
8	Shear plane reflection	Weak, positive, inclined	Ice-stream shearing
9	Deformed reflections below URU	Moderate	Glaciotectonic deformation
10	Seismic anomalies below URU	Strong, negative and positive	Shallow gas accumulations

Table 2

Technology	Frequency [Hz]	Velocity [m/s]	Depth [m]	1st Fresnel Zone [m]	λ/4 [m]
MBE, Reson SeaBat 7111	100,000	1500	450	1.8	0.004
MBE, Kongsberg EM 300	30,000	1500	450	3.4	0.01
Conventional 3D, dominant	45	1500	450	86.6	8.33
P-Cable 3D, dominant*	144	1500	450	48.4	2.60
P-Cable 3D, maximum**	325	1500	450	32.2	1.15
P-Cable 3D, observed***	280	1500	450	34.7	1.34

Bullet points (3-5 BP, max. 85 character per BP)

- High-resolution 3D P-Cable is a useful tool for imaging glacial landforms
- The seismic data allow to study the link between seabed morphology and underlying geology
- A buried shear margin moraine was imaged in the P-Cable data
- Buried glacial horizons can be mapped at MBE-quality using the P-Cable technology
- Meter-scale glacial deposits can be imaged using seismic attribute maps

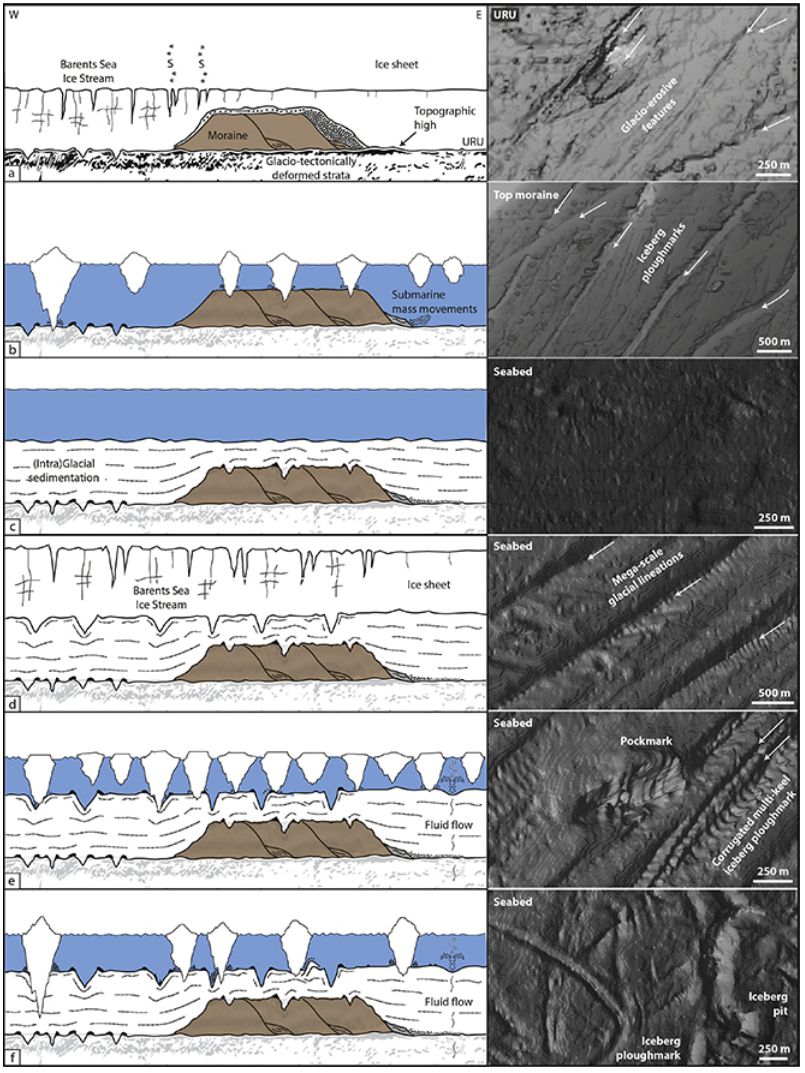

Graphics Abstract

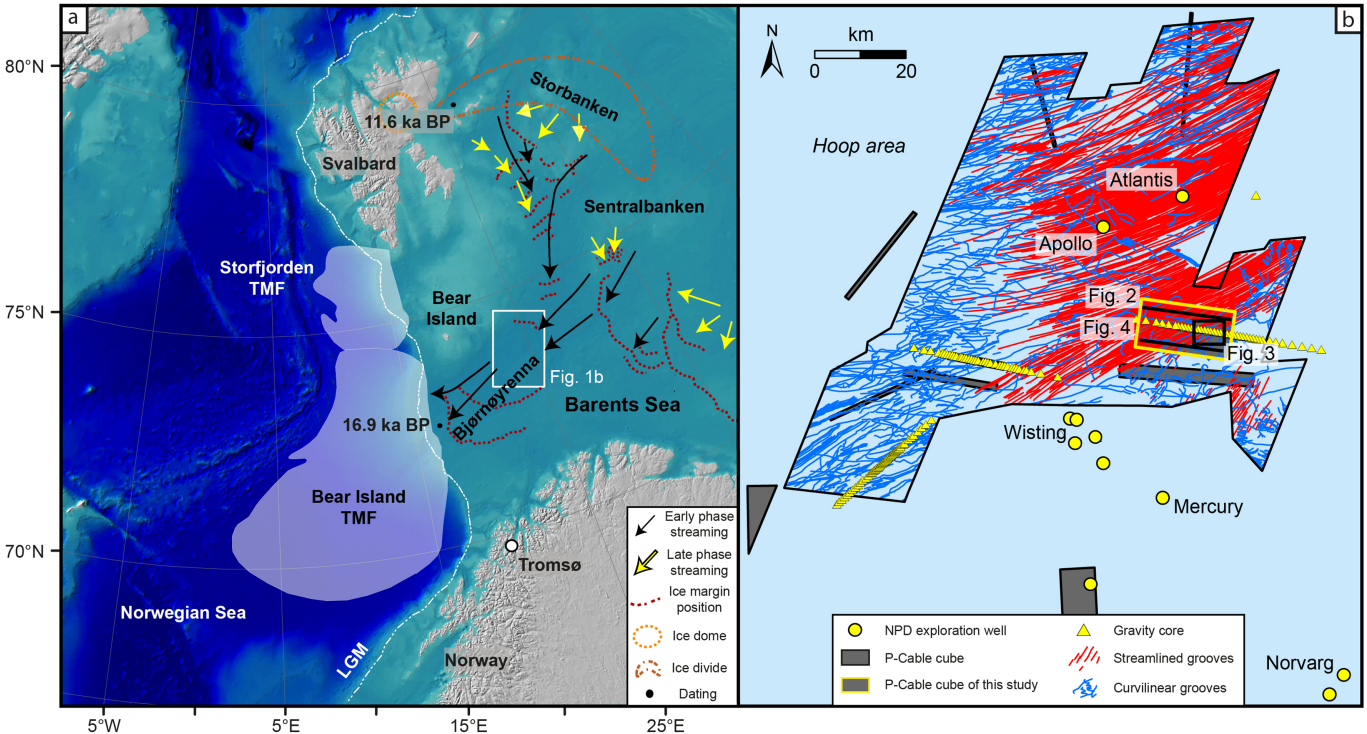
a
b
80°N
75°N
70°N
5°W
5°E
15°E
25°E
11.6 ka BP
Svalbard
Storbanken
Sentralbanken
Storfjorden TMF
Bear Island
Fig. 1b
Barents Sea
Bjørnøyrenna
16.9 ka BP
Bear Island TMF
Tromsø
Norwegian Sea
LGM
Norway
Early phase streaming
Late phase streaming
Ice margin position
Ice dome
Ice divide
Dating
N
km
0
20
Hoop area
Atlantis
Apollo
Fig. 2
Fig. 4
Fig. 3
Wisting
Mercury
Norvarg
NPD exploration well
P-Cable cube
P-Cable cube of this study
Gravity core
Streamlined grooves
Curvilinear grooves

Figure 1

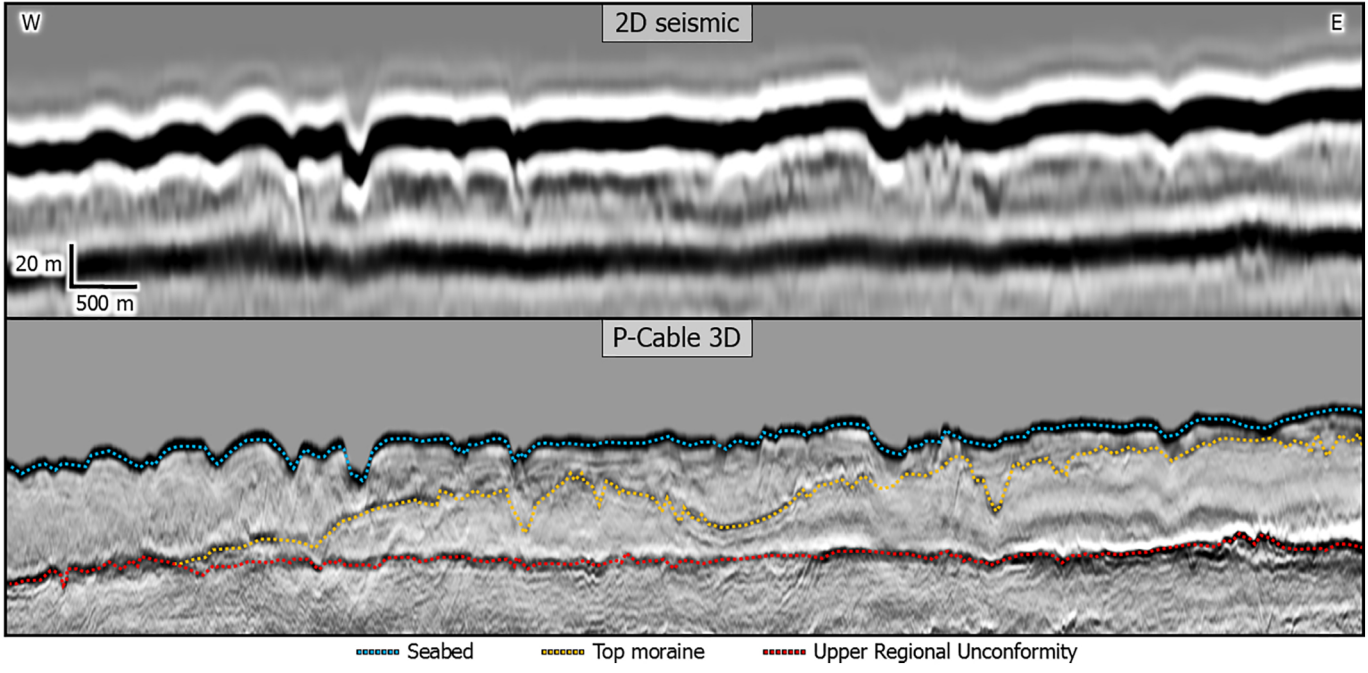
W
2D seismic
E
20 m
500 m
P-Cable 3D
Seabed
Top moraine
Upper Regional Unconformity

Figure 2

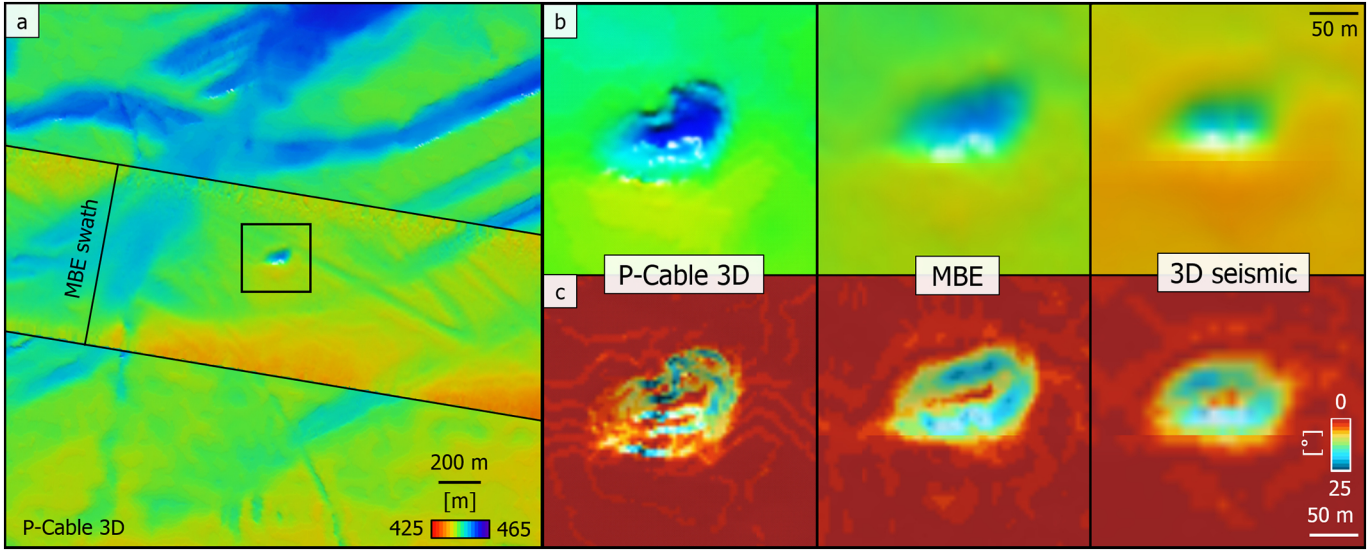
a
MBE swath
200 m
[m]
425
465
P-Cable 3D
b
50 m
P-Cable 3D
MBE
3D seismic
c
0
[°]
25
50 m

Figure 3

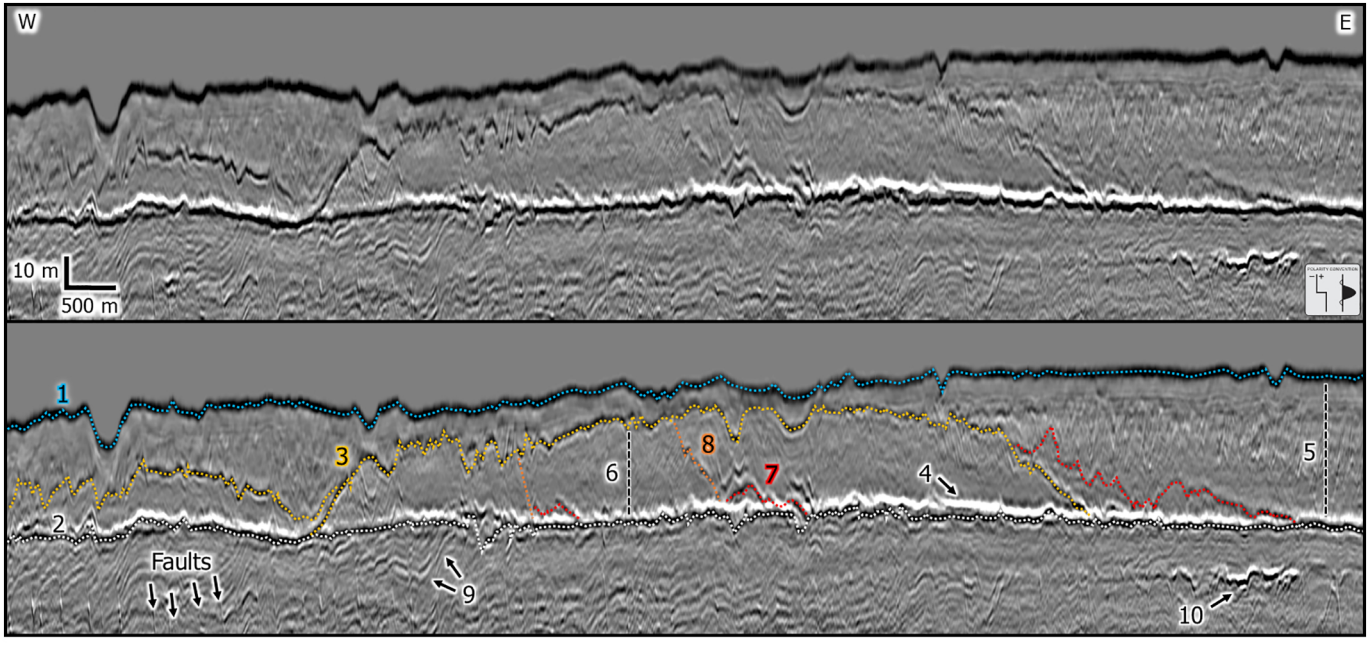
W
E
10 m
500 m
1
2
3
4
5
6
7
8
9
10
Faults
Seabed
Top moraine
Mass Transport Deposits
Shear plane
Upper Regional Unconformity

Figure 4

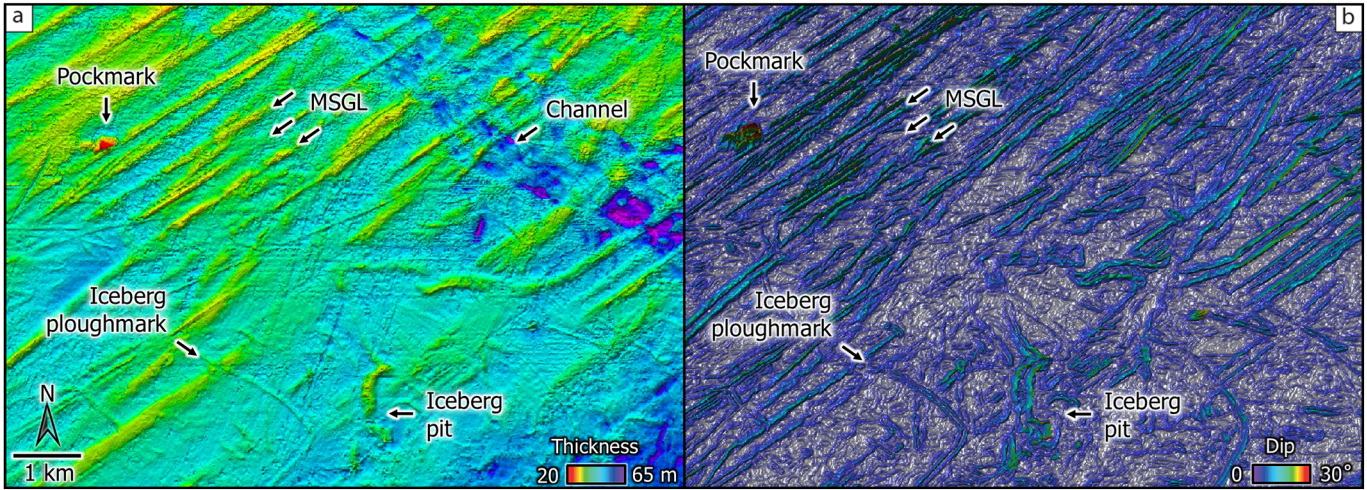
a
Pockmark
MSGL
Channel
Iceberg
ploughmark
Iceberg
pit
N
1 km
Thickness
20
65 m
b
Pockmark
MSGL
Iceberg
ploughmark
Iceberg
pit
Dip
0
30°

Figure 5

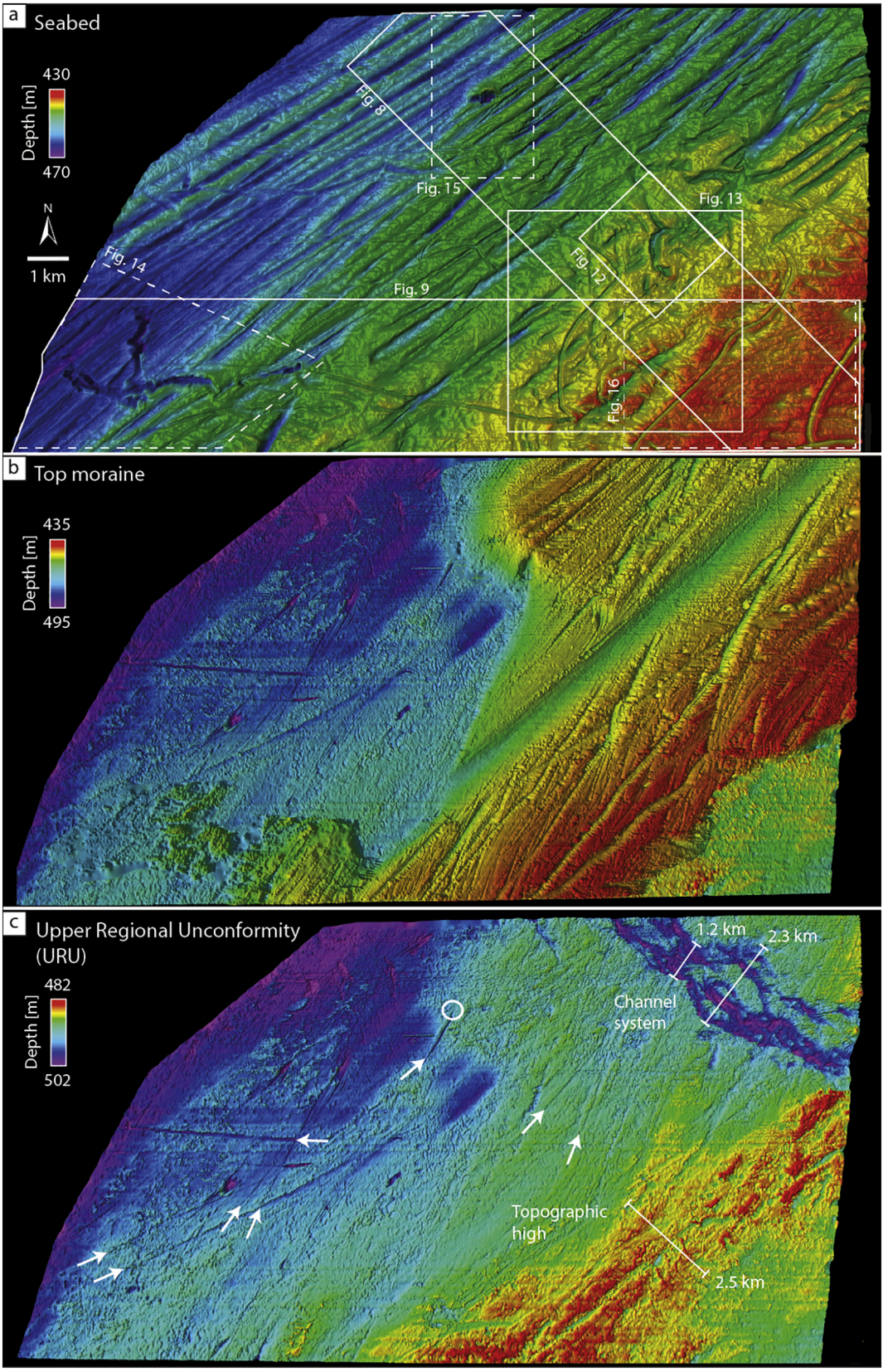
a
Seabed
Depth [m]
430
470
N
1 km
Fig. 8
Fig. 15
Fig. 13
Fig. 12
Fig. 14
Fig. 9
Fig. 16
b
Top moraine
Depth [m]
435
495
c
Upper Regional Unconformity
(URU)
Depth [m]
482
502
1.2 km
2.3 km
Channel
system
Topographic
high
2.5 km

Figure 6

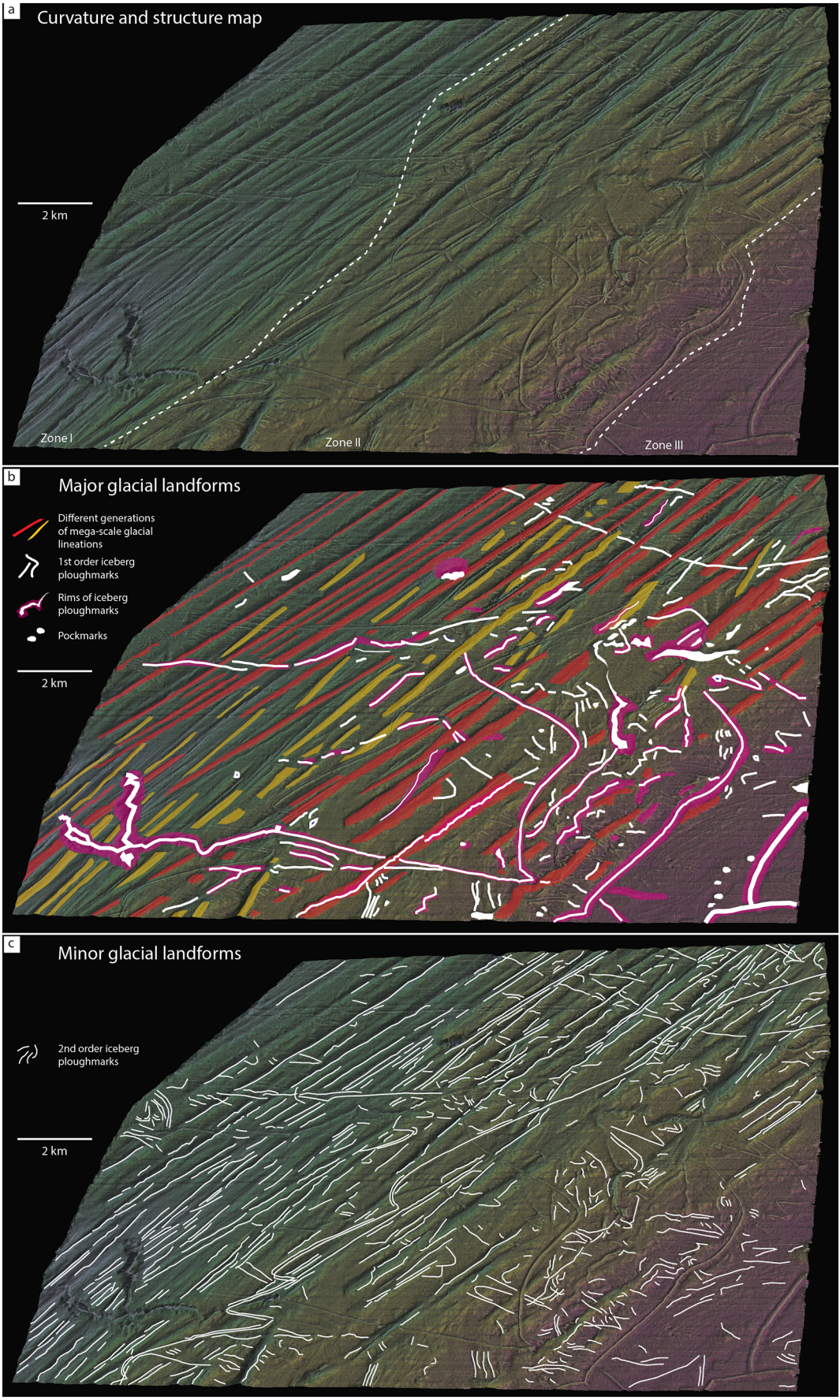
a
Curvature and structure map
2 km
Zone I
Zone II
Zone III
b
Major glacial landforms
Different generations of mega-scale glacial lineations
1st order iceberg ploughmarks
Rims of iceberg ploughmarks
Pockmarks
2 km
c
Minor glacial landforms
2nd order iceberg ploughmarks
2 km

Figure 7

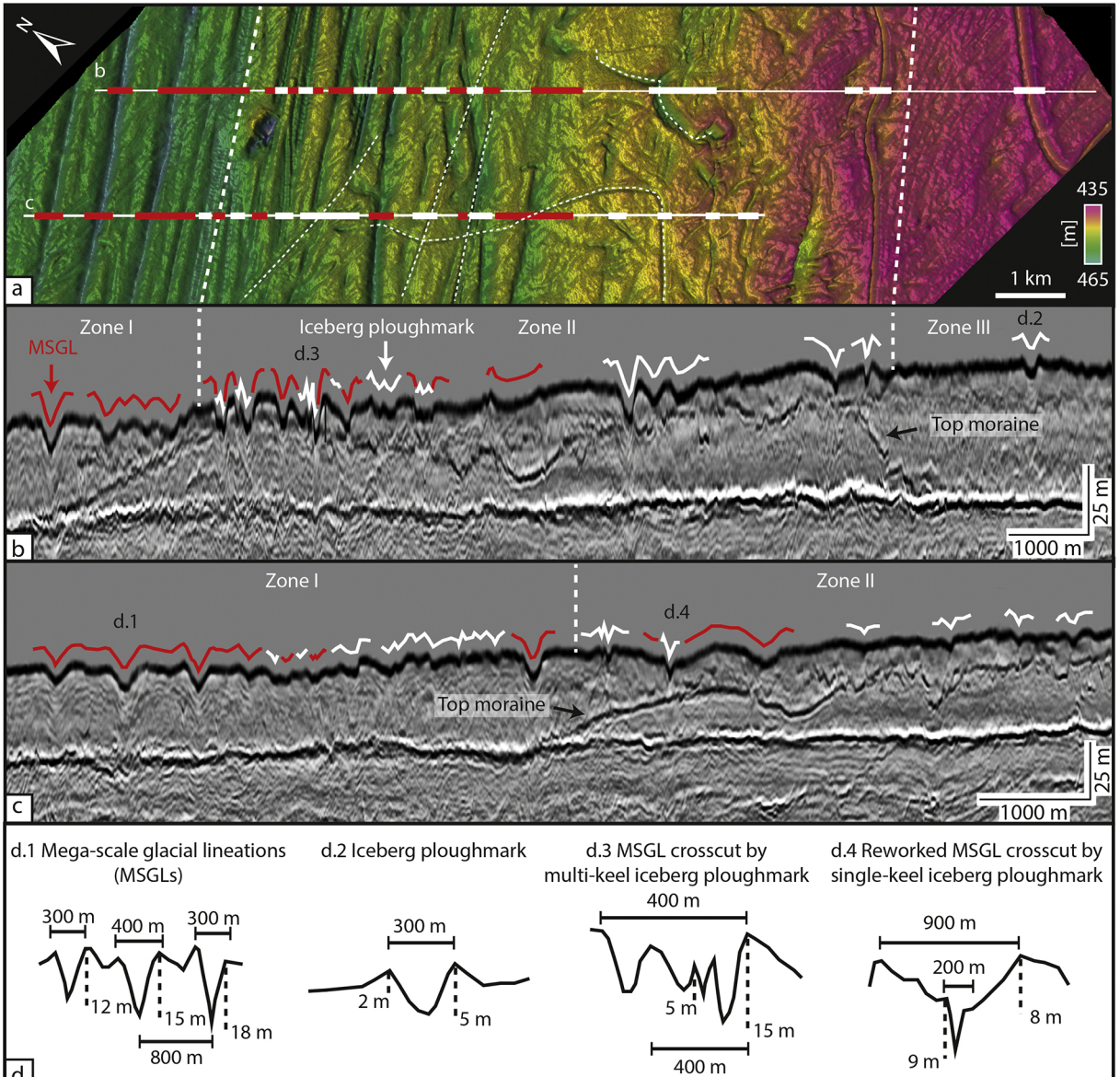
N
b
c
435
[m]
465
1 km
a
Zone I
MSGL
Iceberg ploughmark
d.3
Zone II
Zone III
d.2
Top moraine
25 m
1000 m
b
Zone I
Zone II
d.1
d.4
Top moraine
25 m
1000 m
c
d.1 Mega-scale glacial lineations (MSGLs)
300 m
400 m
300 m
12 m
15 m
18 m
800 m
d.2 Iceberg ploughmark
300 m
2 m
5 m
d.3 MSGL crosscut by multi-keel iceberg ploughmark
400 m
5 m
15 m
400 m
d.4 Reworked MSGL crosscut by single-keel iceberg ploughmark
900 m
200 m
8 m
9 m
d

Figure 8

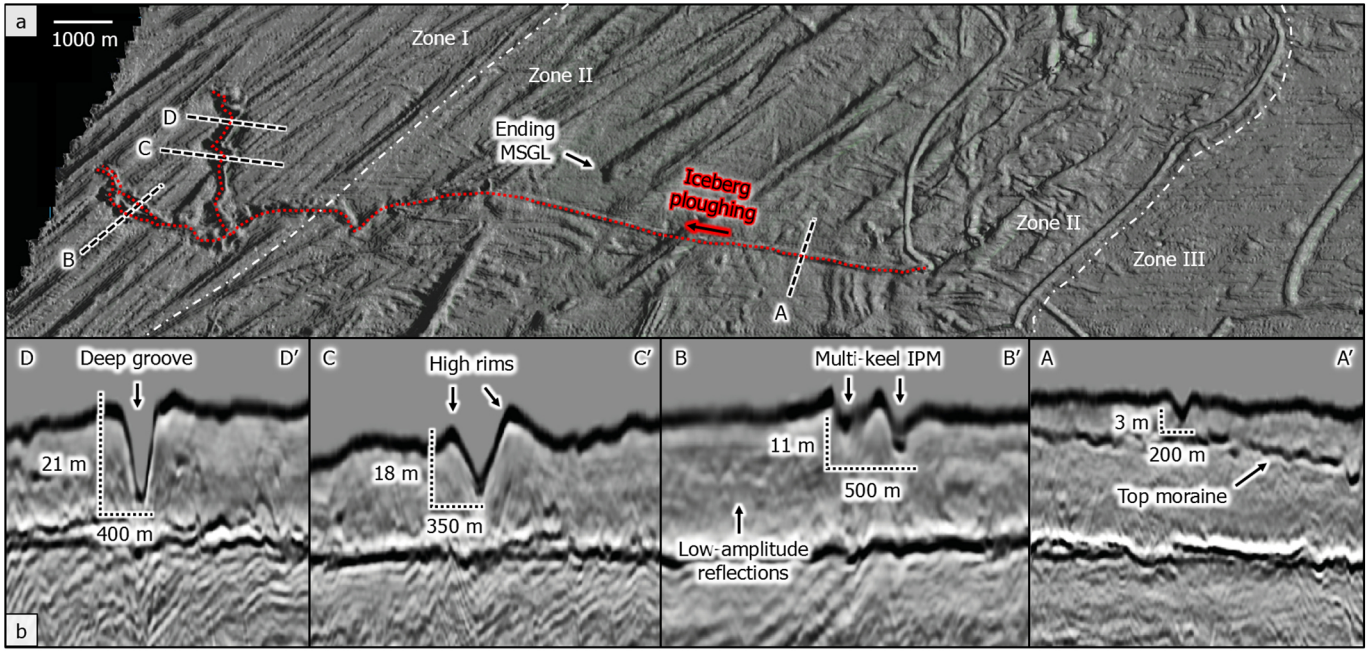
a
1000 m
Zone I
Zone II
Ending
MSGL
Iceberg
ploughing
Zone II
Zone III
D
C
B
A
D
Deep groove
D′
21 m
400 m
C
High rims
C′
18 m
350 m
B
Multi-keel IPM
B′
11 m
500 m
Low-amplitude
reflections
A
A′
3 m
200 m
Top moraine
b

Figure 9

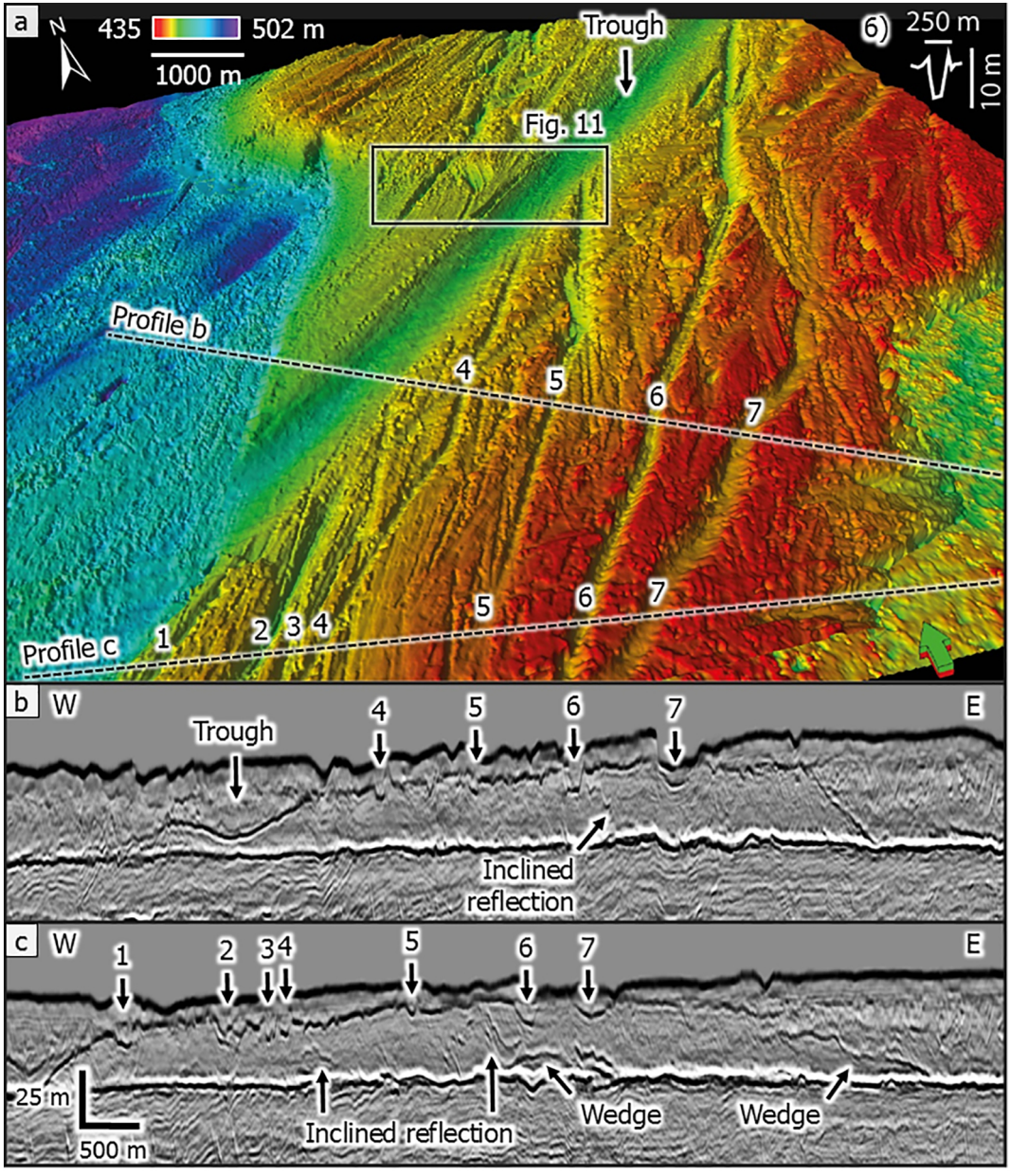
a
N
435
502 m
1000 m
Trough
Fig. 11
6)
250 m
10 m
Profile b
4
5
6
7
Profile c
1
2
3
4
5
6
7
b
W
E
Trough
4
5
6
7
Inclined reflection
c
W
E
1
2
3
4
5
6
7
25 m
500 m
Inclined reflection
Wedge
Wedge

Figure 10

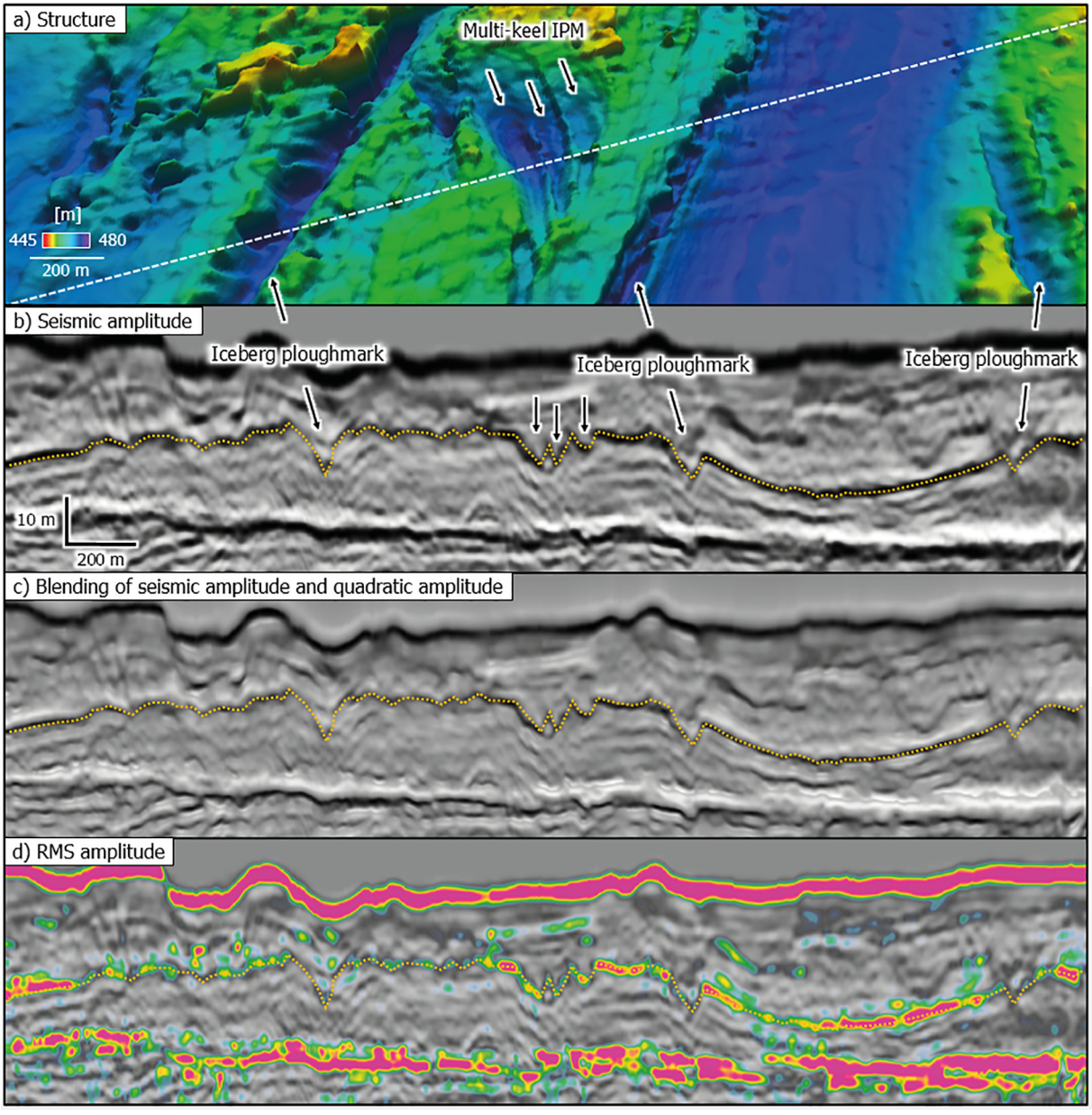
a) Structure
Multi-keel IPM
[m]
445
480
200 m
b) Seismic amplitude
Iceberg ploughmark
Iceberg ploughmark
Iceberg ploughmark
10 m
200 m
c) Blending of seismic amplitude and quadratic amplitude
d) RMS amplitude

Figure 11

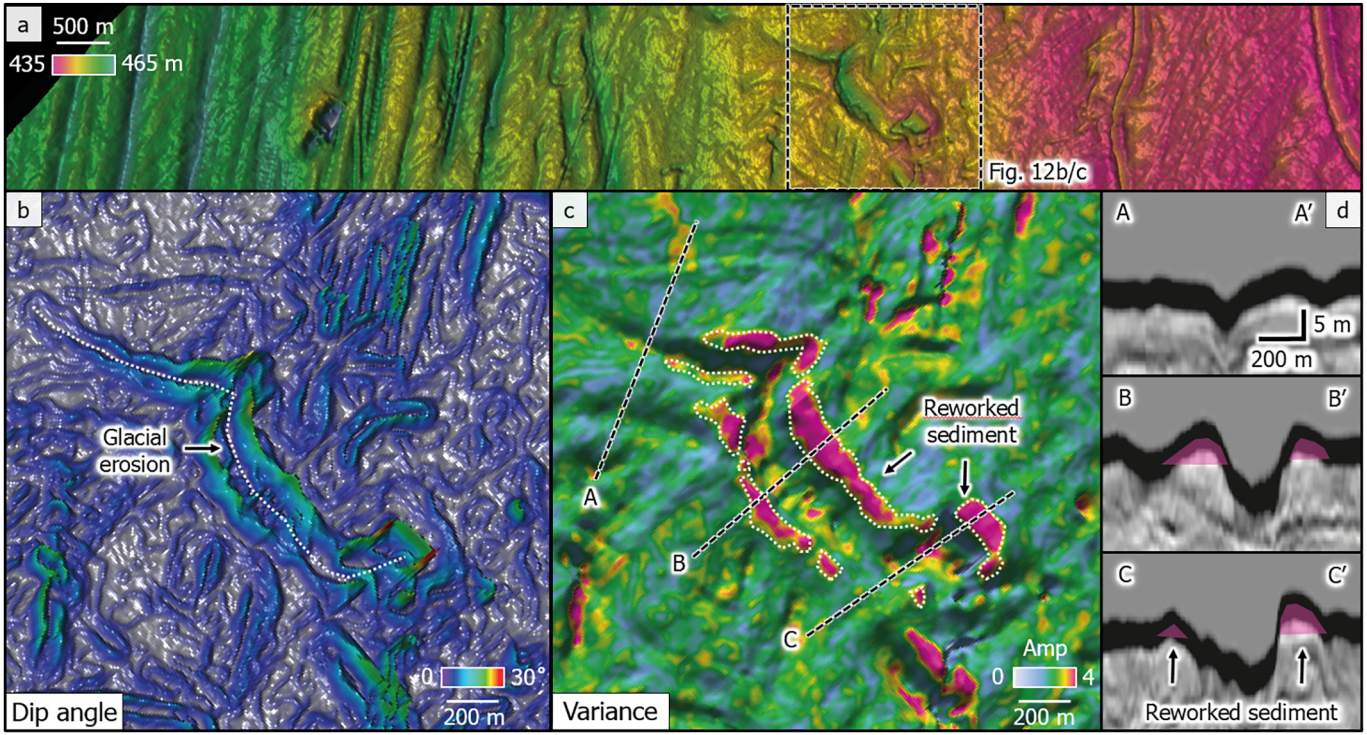
a
500 m
435
465 m
Fig. 12b/c
b
Glacial erosion
0
30°
200 m
Dip angle
c
A
B
C
Reworked sediment
Amp
0
4
200 m
Variance
A
A′
d
5 m
200 m
B
B′
C
C′
Reworked sediment

Figure 12

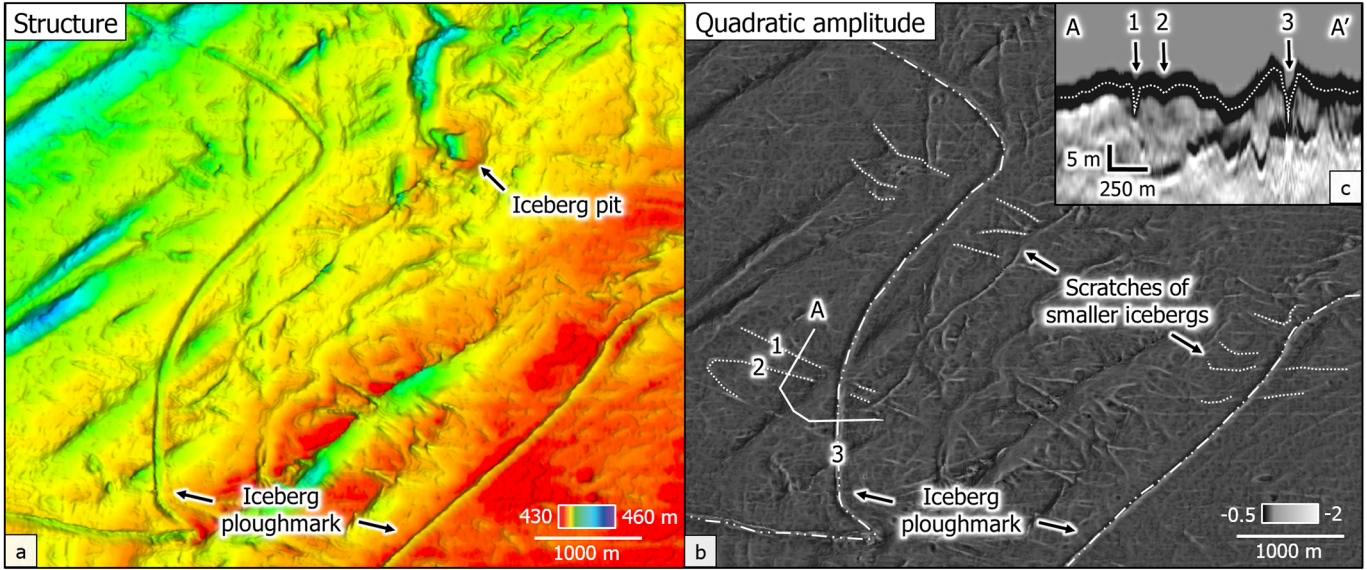
Structure
Iceberg pit
Iceberg ploughmark
430
460 m
1000 m
a
Quadratic amplitude
A
1
2
3
A'
5 m
250 m
c
Scratches of smaller icebergs
A
1
2
3
Iceberg ploughmark
-0.5
-2
1000 m
b

Figure 13

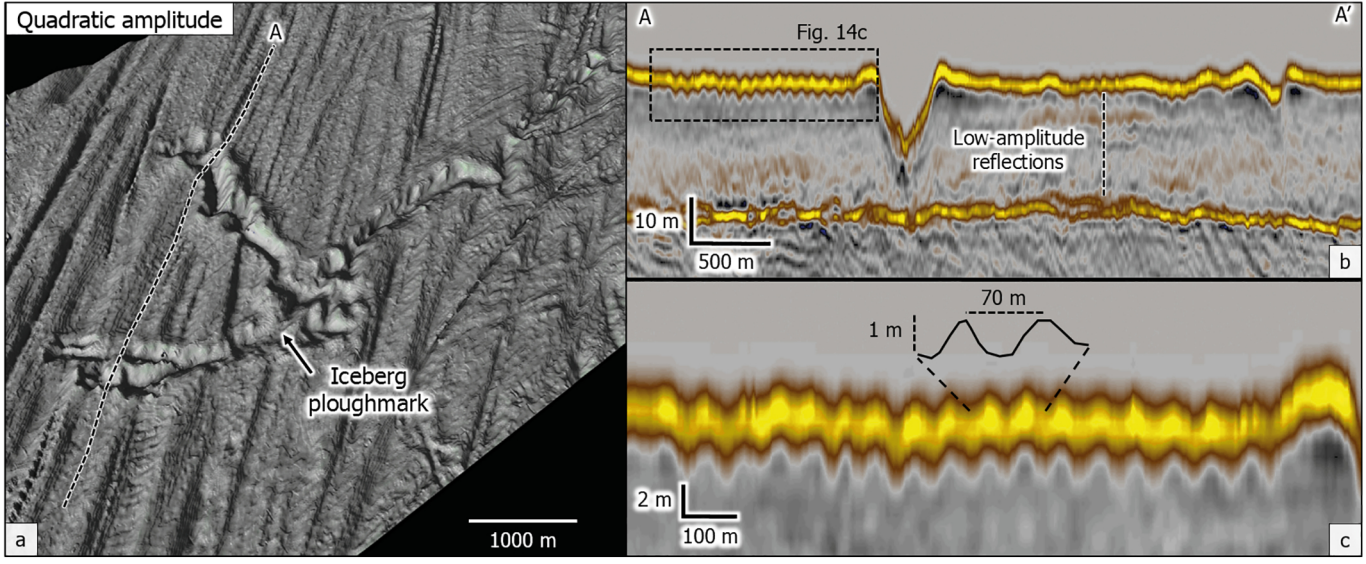
Quadratic amplitude
A
Iceberg ploughmark
1000 m
a
A
Fig. 14c
A'
Low-amplitude reflections
10 m
500 m
b
70 m
1 m
2 m
100 m
c

Figure 14

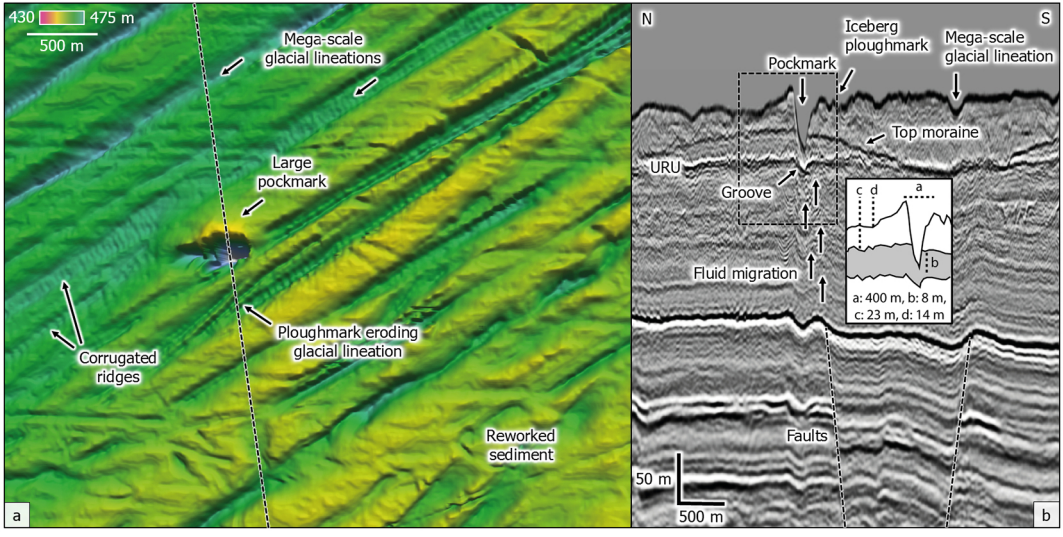
430
475 m
500 m
Mega-scale glacial lineations
Large pockmark
Corrugated ridges
Ploughmark eroding glacial lineation
Reworked sediment
a
N
S
Iceberg ploughmark
Pockmark
Mega-scale glacial lineation
Top moraine
URU
Groove
Fluid migration
c d a
b
a: 400 m, b: 8 m,
c: 23 m, d: 14 m
Faults
50 m
500 m
b

Figure 15

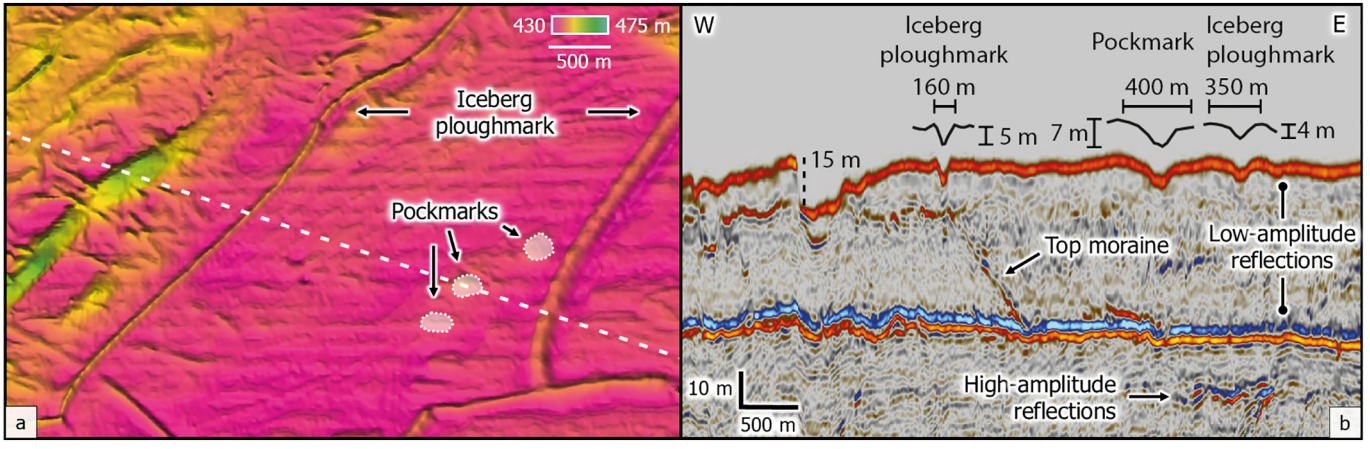
430
475 m
500 m
Iceberg
ploughmark
Pockmarks
a
W
Iceberg
ploughmark
Pockmark
Iceberg
ploughmark
E
160 m
400 m
350 m
5 m
7 m
4 m
15 m
Top moraine
Low-amplitude
reflections
10 m
500 m
High-amplitude
reflections
b

Figure 16

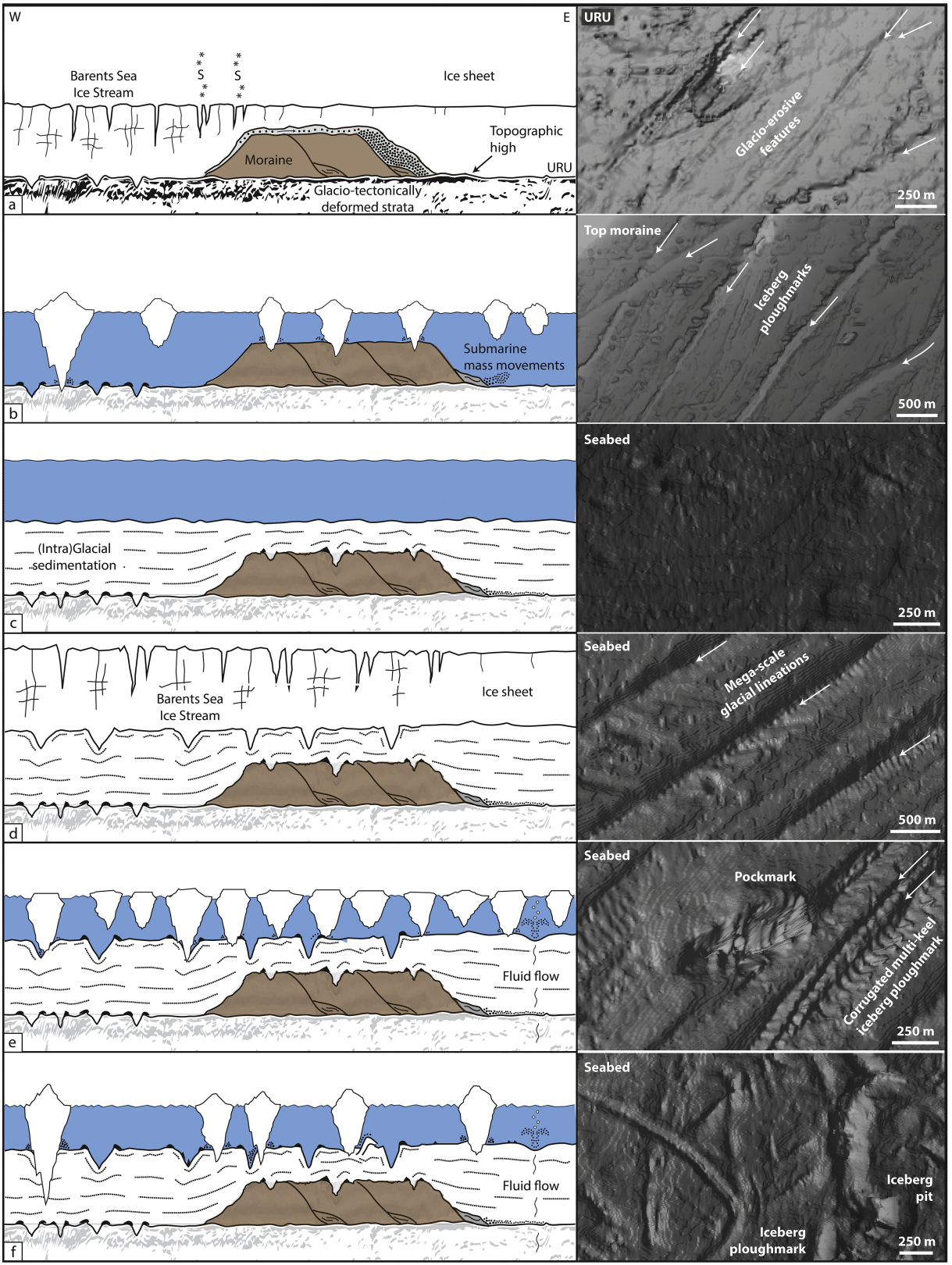
W
E
Barents Sea
Ice Stream
Ice sheet
Topographic
high
Moraine
URU
Glacio-tectonically
deformed strata
a
URU
Glacio-erosive
features
250 m
Top moraine
Iceberg
ploughmarks
500 m
b
Submarine
mass movements
Seabed
250 m
(Intra)Glacial
sedimentation
c
Seabed
Mega-scale
glacial lineations
500 m
Barents Sea
Ice Stream
Ice sheet
d
Seabed
Pockmark
Corrugated multi-keel
iceberg ploughmark
250 m
Fluid flow
e
Seabed
Iceberg
pit
Iceberg
ploughmark
250 m
Fluid flow
f

Figure 17